



HD 145263: Spectral Observations of Silica Debris Disk Formation via Extreme Space Weathering?

C. M. Lisse¹, H. Y. A. Meng², M. L. Sitko³, A. Morlok⁴, B. C. Johnson⁵, A. P. Jackson^{6,7}, R. J. Vervack, Jr.¹,
C. H. Chen⁸, S. J. Wolk⁹, M. D. Lucas^{10,11}, M. Marengo¹⁰, and D. T. Britt¹²

¹ JHU-APL, 11100 Johns Hopkins Road, Laurel, MD 20723, USA; carey.lisse@jhuapl.edu, ron.vervack@jhuapl.edu

² Steward Observatory, Department of Astronomy, University of Arizona, 933 N Cherry Ave, Tucson, AZ 85721, USA; hyameng@gmail.com

³ Department of Physics, University of Cincinnati, Cincinnati, OH 45221-0011 and Space Science Institute, Boulder, CO 80301, USA; sitkomi@ucmail.uc.edu

⁴ Institut für Planetologie, Universität Münster, Wilhelm-Klemm-Straße 9 D-48149 Münster, Germany; morlokan@uni-muenster.de

⁵ Department of Earth, Atmospheric, and Planetary Sciences, Purdue University, 550 Stadium Mall Drive, West Lafayette, IN 47907, USA; bcjohnson@purdue.edu

⁶ Centre for Planetary Sciences, University of Toronto, 1265 Military Trail, Toronto ON, M1C 1A4, Canada; ajackson@cita.utoronto.ca

⁷ School of Earth and Space Exploration, Arizona State University, 781 E Terrace Mall, Tempe, AZ 85287, USA

⁸ Space Telescope Science Institute, 3700 San Martin Dr. Baltimore, MD 21218, USA; cchen@stsci.edu

⁹ Chandra X-ray Center, Harvard-Smithsonian Center for Astrophysics, 60 Garden Street, Cambridge, MA 02138, USA; swolk@cfa.harvard.edu

¹⁰ Department of Physics and Astronomy, 12 Physics Hall, Iowa State University, Ames, IA 50010, USA; mmarengo@iastate.edu

¹¹ Institute for Astronomy, University of Hawai'i at Manōa, 2680 Woodlawn Dr, Honolulu, HI 96822, USA; mdlucas@iastate.edu

¹² Department of Physics, University of Central Florida, Orlando, FL 32816, USA; dbritt@ucf.edu

Received 2019 February 21; revised 2020 February 8; accepted 2020 February 27; published 2020 May 12

Abstract

We report here time-domain infrared spectroscopy and optical photometry of the HD 145263 silica-rich circumstellar-disk system taken from 2003 through 2014. We find an F4V host star surrounded by a stable, massive 10^{22} – 10^{23} kg (M_{Moon} to M_{Mars}) dust disk. No disk gas was detected, and the primary star was seen rotating with a rapid ~ 1.75 day period. After resolving a problem with previously reported observations, we find the silica, Mg-olivine, and Fe-pyroxene mineralogy of the dust disk to be stable throughout and very unusual compared to the ferromagnesian silicates typically found in primordial and debris disks. By comparison with mid-infrared spectral features of primitive solar system dust, we explore the possibility that HD 145263's circumstellar dust mineralogy occurred with preferential destruction of Fe-bearing olivines, metal sulfides, and water ice in an initially comet-like mineral mix and their replacement by Fe-bearing pyroxenes, amorphous pyroxene, and silica. We reject models based on vaporizing optical stellar megafares, aqueous alteration, or giant hypervelocity impacts as unable to produce the observed mineralogy. Scenarios involving unusually high Si abundances are at odds with the normal stellar absorption near-infrared feature strengths for Mg, Fe, and Si. Models involving intense space weathering of a thin surface patina via moderate ($T < 1300$ K) heating and energetic ion sputtering due to a stellar super-flare from the F4V primary are consistent with the observations. The space-weathered patina should be reddened, contain copious amounts of nanophase Fe, and should be transient on timescales of decades unless replenished.

Unified Astronomy Thesaurus concepts: Planetary system formation (1257); Time domain astronomy (2109); Stellar astronomy (1583); Spectroscopy (1558); Circumstellar matter (241); Stellar classification (1589)

1. Introduction

Debris disks are the signposts of terrestrial planet formation and evolution (Zuckerman & Song 2004; Raymond et al. 2011). When giant planet accretion comes to a halt as the primordial disk gas dissipates after the first ~ 10 Myr of star formation (Mamajek 2009; Fedele et al. 2010; Ribas et al. 2015; Meng et al. 2017), solid materials in the remaining disk still grow by colliding and aggregating toward terrestrial planets (Kenyon & Bromley 2005, 2006; Morishima et al. 2010; Chambers 2013; Raymond et al. 2014). This process of “late-stage” terrestrial planet accretion may last upwards of ~ 100 Myr, featuring large-scale, dust-producing impacts between planetesimals and planetary embryos (Kenyon & Bromley 2006, 2016; Genda et al. 2016). Fine dust produced in these large impacts can yield prominent spectral features observable in the mid-infrared. Silicate-emission debris disks have been observed around many young stars (Mittal et al. 2015); temporal variability has confirmed that recent large or giant impacts are indeed the culprits responsible for at least some of them (Meng et al. 2014, 2015).

The past decade has seen the emergence and development of the astromineralogy of dust with emission features based on

Spitzer/IRS (Houck et al. 2004) observations (e.g., Lisse et al. 2006, 2007a, 2007b, 2008, 2009; Reach et al. 2009, 2010; Fujiwara et al. 2010, 2012; Currie et al. 2011; Sitko et al. 2011; Olofsson et al. 2012; Chen et al. 2014; Mittal et al. 2015) but also on data from large ground-based telescopes (e.g., Honda et al. 2004; Rhee et al. 2007, 2008). Mineralogical and chemical information is obtained by matching the linear superposition of laboratory model emissivity spectra to the Spitzer data. In the course of studying 20+ bright dust disk sources, we have noted a range of dust compositions, but find that the large majority of disks are composed of the Fe/Mg olivines, Ca/Fe/Mg pyroxenes, Fe/Mg sulfides, amorphous inorganic carbon, and water ice/gas, found in abundance in comets, asteroids, and KBOs in our solar system.

Lisse et al. (2009) examined the unusual silica-dust rich debris disk found in the HD 172555 system. Found surrounding a young (~ 23 Myr; Mamajek & Bell 2014) A7V star in the Beta Pic moving group, the mid-infrared spectrum of this system obtained by the Spitzer/IRS spectrometer in 2004 showed strong solid-state emission features in the unusual 8–9 μm region, distinctly different from the usual 9–12 μm Si–O stretch features evinced by ferromagnesian olivines and

pyroxenes. Analysis showed that these features were best matched by the emissivity spectra of amorphous silicas, like those found in terrestrial tektites, materials formed by flash re-freezing of rock vaporized in hypervelocity impacts. Given that the HD 172555 system contains no detectable circumstellar gas around the central A7V primary star, which is itself X-ray quiet, they argued that the only possible known mechanism for producing the observed silicas would be from a giant impact between two Mercury-sized (or larger) rocky planetesimals.

In this paper, we discuss five mid-infrared spectral measurements of another system, HD 145263, an F4V star in the ~ 11 Myr old Upper Sco association ($l = 349^\circ.7$, $b = 18^\circ.73$, *Gaia* DR2 distance = 142 pc; Preibisch & Mamajek 2008; Pecaut et al. 2012; Bailer-Jones et al. 2018), which also demonstrates strong 7–8 μm silica emission and 8–13 μm silicate emission features from warm ($T \sim 285$ K) dust at ~ 3 au from the $L = 4.1 L_{\text{solar}}$ primary (Pecaut et al. 2012). HD 145263 is one of seven well known debris disks in our NASA/IRTF northern sky Near InfraRed Disk Systems (NIRDS) survey with very large and structured excess flux at 8–13 μm due to thermal emission from warm (150–400 K) dust in the terrestrial planet zone of their systems (Figure 1; total $F_{\text{IR}}/F_{\text{bol}} \sim 1 \times 10^{-3}$, Chen et al. 2011). Because of its low cluster age, it could harbor a protoplanetary or transition disk; as we find an optically thin disk with no evidence for circumstellar gas emission lines containing very processed dust, we can rule out a protoplanetary disk and must instead be observing a transition disk or very young debris disk. By simple scaling of its mid-infrared (hereafter MIR) flux, the ~ 0.4 Jy at 10 μm circumstellar disk must be massive, on the order of 10^{22} – 10^{23} kg (after allowing for their relative primary luminosities, it must be $\sim 10\times$ more massive than the 29 pc distant HD 172555, which is 1 Jy at 10 μm).

Unlike HD 172555, however, we have five different MIR spectra taken in 2003–2014 to study (Figure 1(a)), allowing us to search for temporal variability in the system. The first published mid-infrared HD 145263 spectrum, taken by Honda et al. (2004) using the ground-based Subaru/COMICS instrument in 2003, did *not* show any evidence of silica dust emission features in our analysis, but instead, appeared to be a good match to the spectra found for dust emitted by active solar system comets. (At ~ 11 Myr age, it was plausible that the star has remnants of its primitive primordial birth disk still orbiting about it, especially since “The F-type members of Upper Sco appear to be all pre-main sequence” according to Pecaut et al. 2012.) The latter three spectra, taken using Spitzer/IRS in 2005, 2007, and 2009, appeared to show a markedly different composition than in 2003, one not reproducible using models of new dust replacement or high-temperature thermal processing. At the same time, the circumstellar-disk-emitted energy, particle size distribution (PSD), and temperature did not appear to have changed much, which initially led us to argue that selective in situ chemical processing of the circumstellar dust, driven by the central star, was at play.

As a check, we later obtained archival Subaru/COMICS spectra of HD 145263 from 2014, in order to secure that the apparent change from 2003 to 2005–2009 was real and not a relative calibration effect between the two different observatories. When we reduced the data, we found good agreement between the 2014 Subaru/COMICS 8–13 μm spectrum and the corresponding part of the Spitzer/IRS 2005–2009 spectra, obviating any calibration issues between the two data sets.

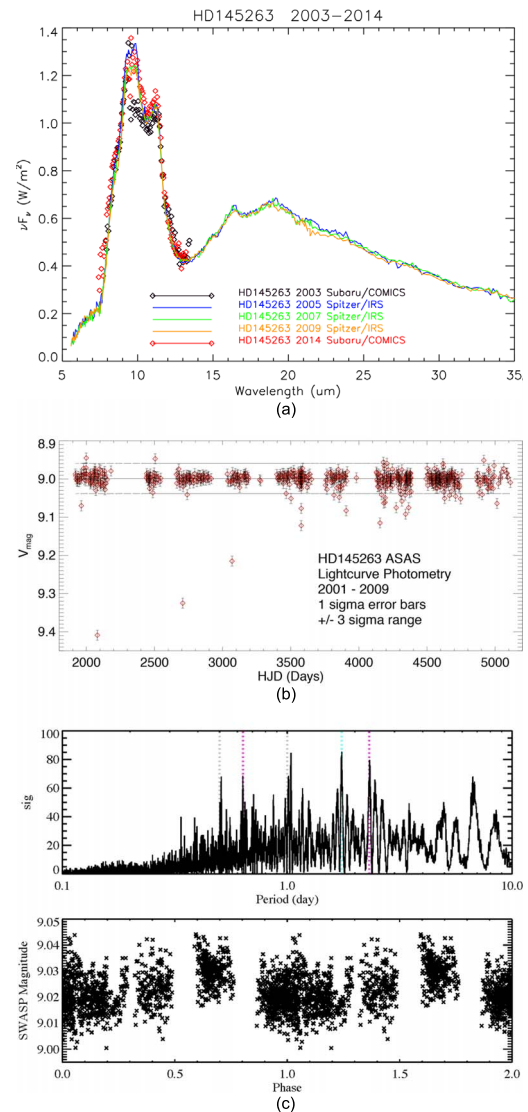


Figure 1. Panel (a): comparison of the revised 2003 Subaru/COMICS HD 145263 observation in 2003 (originally published in Honda et al. (2004) and corrected in this work; black diamonds) to the Spitzer/IRS spectra from the 2005 through 2009 epochs (blue/green/yellow). For clarity, error bars are not plotted. Also shown is the Subaru/COMICS HD 145263 observation of Fujiwara et al. (2013; red diamonds). Error bars have been suppressed to allow direct comparison of the agreement between the different spectra. The errors in an individual visit can be estimated from the scatter in the data, and the relative errors between repeated visits from each telescope average 10%. The absolute calibration difference between the Subaru and Spitzer data sets averages 30% due to differences in the effective beam size of each slit, with the Subaru measured Jy being 1.3 times higher than the reported Spitzer spectral fluxes. After correcting the Subaru data to match the Spitzer calibration as shown, the total 8–13 μm emitted radiance for the system is found to vary by less than 10%. Panel (b): long-term V-band photometry for HD 145263 from the ASAS website (<http://www.astrouw.edu.pl/asas/?page=aase>) spanning 2001 January 1 (HJD = 2451910.5) to 2009 October 10 (HJD = 2455105.5). Subaru/COMICS observed the system on JD 2452835.5 (2003 July 15) and the first Spitzer/IRS observation occurred on JD 2453444.5 (2005 March 15). There are three single-point measurements in this interval differing by somewhat more than 3σ from the $V = 8.99$ temporal median that would be indicative of long-term stellar flaring; for 622 measurements, we expect 1.7 for normally distributed statistics. There are multiple epochs of single-point excursions much fainter than the $V = 8.99$ temporal median by up to 0.40 mag, but they are not reproduced by neighboring samples, and it is not clear whether they represent real changes in the system’s visual output or simply noisy data dropouts. Panel (c): SigSpec periodogram of the filtered superSWASP time series obtained between 2006 July 5 and 2008 August 8. (Top panel) The power spectrum. The strongest signal has a period of 1.747 ± 0.001 days, with aliases peaking near 0.64 and 2.31 days. Artifacts associated with the observational cadence can be seen near 0.5, 1.0, and 6.67 days. (Bottom panel) The HD 145263 superSWASP phase curve folded with the 1.747 day period.

However, when we applied the same data reduction methodology to the Subaru/COMICS 2003 data of Honda et al. as a further check, we could not reproduce the spectrum published in Honda et al. (2004), but instead found a spectrum consistent with the four other 2005–2014 spectra. We have thus obviated any rapid change occurring in the system’s dust disk between 2003 and 2005. One of the most important goals for this paper is to set the literature record straight, in that what had appeared to be a pronounced change in the spectral character of the system’s debris disk dust from 2003 to 2005 (in less than 2 yr!) has become instead 11 yr of a spectrally stable silica-rich debris disk.

Our initial work pursuing a rapid central-star driven metamorphosis of HD 145263’s debris disk was not in vain, though, because in doing so, we researched plausible non-impact-driven physical mechanisms for producing a mixture of reduced, low-temperature ferromagnesian pyroxenes + silica. One of these mechanisms, giant stellar XUV “space-weathering” alteration of dust particle surfaces in an initially primitive comet-dust-like circumstellar population, matches very well with what is seen, and we thus report here mineralogical evidence for massively space-weathered circumstellar-disk dust in the HD 145263 system. This was likely created by a giant primary star stellar flare (rather than an abnormally high stellar wind flux; at ~ 11 Myr age, the primary star is also likely still highly active and flaring), and if so, we predict that the effects of this space weathering should grind down on timescales of decades, revealing a more primitive, less processed mix of the “typical” ferromagnesian olivines + pyroxenes seen in young debris disks.

2. HD 145263 System Observations and Gross Characterization

The mid-infrared spectroscopic data we used for characterizing the HD 145263 system are the 2003 ground-based Subaru/Cooled Mid-Infrared Camera and Spectrometer (COMICS) 7.9–13.2 μm spectrum obtained by Honda et al. (2004), the archival 5.3–38 μm Spitzer/InfraRed Spectrograph (IRS) spectra obtained in 2005, 2007, and 2009, and the 2014 archival 7.9–13.2 μm Subaru/COMICS HD 145263 spectrum taken by Fujiwara et al. (2013). In the 2001–2009 timeframe, white-light optical photometry from All-Sky Automated Survey (ASAS; Paczynski 2000; Pojmanski 2002; Pojmanski & Maciejewski 2004) and white light by the Wide Angle Search for Planets (superWASP, Butters et al. 2010) was also obtained to monitor the system’s variability. To bridge the two wavelength regimes, our group obtained 0.8–5.0 μm spectra using the NASA/IRTF SpeX instrument in 2011–2013. For all of the observations, the system was unresolved, and the spectrophotometry represents the total flux emitted from the system of central star + circumstellar disk. The observational data sets used are summarized in Table 1.

2.1. Spitzer Observations

For the Spitzer/IRS 5.3–38 μm data, we first adopted the data products reduced by the optimal extraction in the CASSIS project (Lebouteiller et al. 2011, 2015), which utilize the latest Spitzer mission absolute calibration appropriate for point sources. The spectra then went through an iteration to reject the spectrophotometry at all wavelengths with signal-to-noise ratio below three. To take care of the order-to-order calibration uncertainties, we forced the total fluxes over the overlapped wavelengths between adjacent orders to agree to the short

wavelength values. Finally, the high-resolution spectrum in 2005 was smoothed to the wavelength grid of the low-resolution data. Since none of the spectroscopic observations has contemporary imaging by IRS Peak-up or MIPS, we did not additionally calibrate the spectra to any photometry. The homogeneous data reduction should best preserve the flux information and ensure the direct comparability of the results from different epochs.

2.2. Subaru Observations

To reduce the Subaru/COMICS 7.9–13.2 μm data, we used the specialized software package *q_series* (version 4.2) with identical procedures applied to both epoch’s data sets. (Details of the reduction methodology can be found in the Subaru Data Reduction Cookbook: COMICS (Ray S. Furuya 2012; https://subarutelescope.org/Observing/DataReduction/Cookbooks/COMICS_CookBook2p2E.pdf.) HD 145263 was observed twice by Subaru over 11 yr, on 2003 July 15, and 2014 June 4, respectively. In addition to the spectroscopic data, photometric imaging observations were obtained at two wavebands with the F05C08.70W0.80 ($\lambda \sim 8.8 \mu\text{m}$) and F09C12.50W1.15 ($\lambda \sim 12.4 \mu\text{m}$) filters in 2003. In 2014, the same red filter (F09C12.50W1.15) was used with a different short-wavelength filter, F22C08.60W0.43 ($\lambda \sim 8.6 \mu\text{m}$).

For the spectra, we first averaged the dark-field images and subtracted them from the dome flat field. The result was then convolved with a 20 pixels Gaussian kernel. The final flat field was made by dividing the convolved image by the original. Meanwhile, the averaged dark field was also removed from the object images. Next, the images were corrected for readout noise pattern and flat field, orthogonalized and fitted for a linear wavelength dispersion function, and used to subtract the residual sky pattern along the spatial axis. The outcomes were one science image for each pointing position with a positive spectrum from the odd chopping positions and a negative one from the even positions with an offset in the spatial axis. To measure the spectra, both the positive and the negative signals were extracted with an aperture width of 9 pixels. The noise level was estimated with two 9-pixel-wide sky windows above and below the spectra, away from any image artifacts. The final spectrophotometric measurements were obtained as the weighted average of all extracted spectra of HD 145263.

The photometric images and standard star observations were prepared with regular dark subtraction and flat field correction. The chopping-nodding strategy commonly used in ground-based mid-IR observations should have, in theory, removed all sky photons. Therefore, we assumed sky brightness of 0 and adopted a radius of 6 pixels for aperture photometry. As a sanity check, we used a sky annulus of 15–30 pixels in radius around HD 145263 and found the average sky brightness fairly close to 0, with deviations slightly larger than the noise at a smaller scale (5×5 pixels), possibly due to some weak, medium-scale dark/flat field residual pattern. Following Honda et al. (2004), we fitted a linear equation for airmass and instrument efficiency effects by matching the observed spectra of the standard stars to their photometry with the two filters used in each observations. The resulting linear equation was then applied to the spectrum of HD 145263 for flux calibration. The calibrated Subaru spectra of HD 145263 in 2003 and 2014 are shown in Figure 1.

Our data reduction and calibration methodology produced a close match between the 2005–2009 Spitzer/IRS mission

Table 1
Program Observations of the HD 145263 Debris Disk

Source	Telescope/Instrument	AOR	λ (μm)	Observation Time (UTC)	BMJD_TDB	Mode
HD 145263	ASAS		0.55	2001 Jan 1–2009 Oct 1		
	SuperWASP		0.55	2006 Jul 5–2008 Aug 8		
	Subaru/COMICS		7.9–13.2	2003 Jul 15	52835.3	
	Subaru/COMICS		7.9–13.2	2014 Jun 4	56812.5	
	Spitzer/IRS	11196928	5.3–37.2	2005 Mar 15	53444.4	SL+SH+LH
	Spitzer/IRS	21808896	5.3–38	2007 Sep 4	54347.9	SL+LL
	Spitzer/IRS	26316288	5.3–38	2009 Apr 18	54939.6	SL+LL
	ALLWISE		3.35, 4.60, 11, 22	2010 Feb 24	55251.5	Photometric Skyscan
	IRTF/SpEX		2.4–5.0	2011 Apr 21	55672.5	LXD
			0.8–2.4	2013 Jun 8	56451.5	SXD
	Spitzer/IRAC		3.55, 4.49	2013 Apr 28–2013 Nov 14	56410.5–56610.5	Warm Spitzer Photometry

calibrated spectra and the 2003/2014 Subaru/COMICS spectra, giving us confidence in our analysis technique. What we did not find was the marked difference between the 2003 Subaru/COMICS spectrum apparent from comparing the HD 145263 spectrum reported by Honda et al. (2004) and the archival Spitzer data, alleviating any need to explain a marked, rapid spectral change in the disk’s spectral character in the 2 yr between 2003 and 2005. In reconciling the qualitative discrepancy between the results from our reduction of the 2003 data, we have contacted Dr. Honda, who found an error in the stellar photometry used in the 2004 paper, which, if corrected, would lead to essentially the same result with our new re-reduction (M. Honda 2020, private communication).¹³

2.3. ASAS and SuperWASP Observations

The five Subaru/COMICS + Spitzer/IRS spectra are shown together in Figure 1(a), to demonstrate how stable the spectral character was between 2003 and 2014. At the same time, weekly long-term photometric monitoring of HD 145263, in V band by the ASAS 10” telescopes in Las Campanas, Chile and Haleakala, HI (Paczynski 2000; Pojmanski 2002; Pojmanski & Maciejewski 2004) and in white light by superWASP (Butters et al. 2010) detected no significant variation of HD 145263’s brightness. The 2001–2009 V-band photometry for HD 145263

from the ASAS website (<http://www.astrouw.edu.pl/asas/?page=aasc>) is reproduced in Figure 1(b). There are no obvious significant brightening events seen that would be indicative of long-term stellar changes or intrasystem increases in stellar extinction. Whatever may have happened in the pre-2003 timeframe to alter the dust disk material, it must have occurred before 2001 or quickly enough between 2001 and 2003 to avoid ASAS detection, or had no detectable optical counterpart. Steady-state behavior of the system was also found in the 2013 Spitzer 3.6/4.5 μm photometric lightcurves of HD 145263 taken by Meng et al. (2015; see Table 1), who concluded that no detectable long-term temporal trends were occurring in the system during their 10-month-long observational window.

Although the ASAS data had a longer time baseline on HD 145263 (689 measurements in 3192 days), the 2006–2008 superWASP monitoring was much more intensive (5512 measurements in 692 days) and more suitable for stellar periodicity analysis use. After filtering out nights with large internal measurement scatter inconsistent with the ASAS data, we used 1380 measurements in 25 good photometric nights over a baseline of 449 days and the SigSpec algorithm of Reegen (2007), a formal extension of the classical Lomb-Scargle, to analyze the filtered time series data. After ignoring observing cadence artifacts at 0.5, 1.0, and 6.67 days and aliases at 0.64 and 2.31 days, the periodogram (Figure 1(c)) shows a significant period of 1.747 ± 0.001 days with an amplitude of 0.005 ± 0.001 mag, reasonable values for a young, ~ 11 Myr old mid-F star.

If this quick rotational period reflects the equatorial rotation of HD 145263, then assuming a stellar radius of $1.55 R_{\odot}$ suitable for an F4 dwarf (Table 2), we have a linear equatorial surface speed of $v = 45 \text{ km s}^{-1}$. Based on their visual HD 145263 spectroscopy, Chen et al. (2011) measured a projected rotation speed for the star of $v \sin i = 40 \pm 3 \text{ km s}^{-1}$. Equating these two estimates, we can solve for the sky inclination of the stellar equator, and find $i = 63^{\circ (+10)}_{(-8)}$, (where $i = 0^{\circ}$ is pole-on and $i = 90^{\circ}$ is edge-on to the LOS). The HD 145263 circumstellar dust disk should have a similar inclination if it is coplanar with the primary’s equator, implying that we are seeing the disk closer to edge-on than face-on, but still quite tilted upwards away from any problematic edge-on optically thick observing geometry. We should thus be able to observe changes in the disk’s dust, if any, using unresolved spectroscopic measurements.

¹³ To be fair, the stellar photometry for HD 145263 and nearby field stars has been updated since 2003, and the 2003 Subaru/COMICS data is of somewhat lower quality than the 2014 data; i.e., the total on-target integration time in 2003 is much shorter (2160 s versus 6664 s), leading to a slightly lower signal-to-noise ratio than in 2014. Also, no corresponding flat field was taken on the night HD 145263 was observed in 2003. We had to use the flat from the previous night, which provided less than ideal correction. Finally, 21 out of 24 spectroscopic images of HD 145263 in 2003 contained a bright ghost image. The position of the ghost moved from image to image, sweeping through a vast range in the spatial axis. To check the severity of the problem, we tried to only use the three ghost-free images but still got essentially the same spectrum. The ghost-contaminated images were valid in our case probably because we had visually inspected each image and carefully avoided the affected area with some margin when selecting the spectrum- and sky-extraction apertures. On the other hand, Watson et al. (2009), in performing their Spitzer/IRS study of PMS stars in Taurus, found that the shape of Spitzer 8–13 μm spectral features often differed from the Subaru/COMICS measurements, most likely due to problems observing with a warm telescope through the Earth’s atmosphere and in estimating and removing the underlying continuum emission with the limited and noisy baseline available in the COMICS data. (The Watson group is also the source of the three CASSIS HD 145263 Spitzer spectra used in this study.) Other groups have reported disagreements between IRS data and ground-based data (e.g., IRS versus BASS spectra, Kraus et al. 2013). However, our own more recent work with reducing Subaru/COMICS spectra for exodisks and comets has shown its calibration to be reasonable within $\sim 15\%$ relative spectral error, similar to the 10%–15% error quoted for the Spitzer/IRS data.

Table 2
Properties of Star HD 145263 (IRAS F16078-2523; HIP 79288; SAO 184196)^a

Name	Spectral Type	T_* (K)	M_* (M_\odot)	R_* (R_\odot)	L_* (L_\odot)	P_{rot} (days)	d (pc)	Age (Myr)	$f_{\text{IR}}/f_{\text{bol}}$ ^b	T_{dust} (K)	r_{dust} ^c (au)	v_{dust} ^d (km s^{-1})	$P_{\text{orb,dust}}$ (yr)
HD 145263	F4V (F3–F5)	6800 to 6500	1.45 to 1.36	1.58 to 1.49	4.5 to 3.7	1.74 to 1.75	~142	~11	$\sim 1 \times 10^{-3}$	285	~3.0	20.6	4.1

Notes.

^a ZAMS stellar data from Pecaut et al. (2012), Pecaut & Mamajek (2013), and http://www.pas.rochester.edu/~emamajek/EEM_dwarf_UBVIJHK_colors_Teff.txt.

^b From Chen et al. (2011), and estimated using $f_{\text{IR}}/f_{\text{bol}} = 1 \times 10^{-3}$ for A7V HD 17255, then scaling by $1 \times 10^{-3} * (0.5 \text{ Jy}/1.0 \text{ Jy}) * (142 \text{ pc}/29 \text{ pc})^2$.

^c Assuming $T_{\text{dust}} = 282 L^{1/4}/r^{1/2}$.

^d For dust @ 3 au and $M_* = 1.4 M_\odot$, $v = \sqrt{GM_*/r} = \sqrt{G * 1.4 M_\odot/3 \text{ au}} = \sqrt{GM_\odot/2.1 \text{ au}} = 29.8/\sqrt{2.1} \text{ km s}^{-1} = 20.6 \text{ km s}^{-1}$.

2.4. SpeX Observations

In 2011 and 2013, we returned to HD 145263 using the NASA IRTF/SpeX 0.8–5.2 μm spectrometer, in order to further characterize the system as part of our 60+ object NIRDS exodisk/exoplanet spectral survey (Lisse et al. 2015, 2017b, 2017c). The system was observed in two separate runs due to time limitations (with the longer 2.4–5.2 μm integration performed first) but using the same stable A0V calibrator star for both runs. The IRTF/SpeX data are shown as a combined SED with the 2009 Spitzer/IRS data in Figure 2(a), and in detail in Figures 2(b)–(e), to demonstrate that the primary star matches an F4V PHOENIX solar abundance stellar photospheric model (Husser et al. 2013) to a high degree from 0.8 to 3.5 μm . At longer wavelengths (3.5–5.0 μm in the SpeX data, and from 5.3 to 37.2 μm in the Spitzer/IRS data), the observed spectrum deviates above the PHOENIX continuum (i.e., demonstrates a “flux excess”) due to thermal emission from copious orbiting warm ($T \sim 285 \text{ K}$) circumstellar dust. Based on our spectral classification experience with other NIRDS stars, a conservative range for the type of the HD 145263 primary is F3–F5 V (i.e., $F4 \pm 1 \text{ V}$). We use this conservative type range, along with the model stellar properties data published by Pecaut et al. (2012) and Mamajek (2009) (http://www.pas.rochester.edu/~emamajek/EEM_dwarf_UBVIJHK_colors_Teff.txt) to list the primary’s properties in Table 2. It is worth noting that our SpeX F4V determination is in relatively good agreement with stellar properties for HD 145263 based on *Gaia* DR2 spectroscopic observations (Andrae et al. 2018): $T_{\text{eff}} = 6606 \text{ K}$, $A_G = 0.72 \text{ mag}$ (extinction in *Gaia* *G* band, not *V* band), stellar radius 1.56 R_\odot , and luminosity 4.20 L_{es} .

Figure 2(a) also shows that of all of the warm disk systems we have studied, the 8–13 μm “silicate emission complex” of HD 145263 best matches that of transition disk $\sim 10 \text{ Myr}$ old HD 166191 (Kennedy et al. 2014), strongly suggesting we are looking at transition disk behavioral effects in HD 145263. It is also interesting to note that the HD 23514 and HD 15407A spectra form another group of similar silica-rich dust disk spectra, and HD 172555 yet another. We will return to the possibility that this implies multiple mechanisms for forming silica in circumstellar disks in Section 5.

Figures 2(b)–(e) show that HD 145263 evinces no strong lines due to circumstellar CO gas at 2.3–2.5 μm , photospheric accretion (HBr γ or H₂ S(0)), outflowing stellar winds (He I or Fe II), or close-in sublimating dust. If HD 145263 is indeed a transition disk, it is a gas-poor or gas-free one.

3. Circumstellar Dust Mineralogical Modeling

3.1. Methodology

Spectral modeling was carried out by adopting a collection of possible mineralogical species and fitting various composite spectra to the observations. For an optically thin debris disk, a composite spectrum can be written as the combination of the contributions from individual species (Lisse et al. 2009),

$$F_\nu = \frac{1}{\Delta^2} \sum_i \int_{a_{\text{min}}}^{a_{\text{max}}} B_\nu [T_i(a, r)] Q_{\text{abs},i}(a, \lambda) \pi a^2 \frac{dn_i(r)}{da} da$$

where Δ is the distance between the observer and the dust, B_ν is the Planck function at wavelength λ and temperature T , which is dependent on the particle radius a and the i th composition at a distance r from the central star, Q_{abs} is the emission efficiency of the particle, and dn/da is the differential PSD. Our spectral analysis consists of calculating the emission flux for a model collection of dust, and comparing the calculated flux to the observed flux. The emitted flux depends on the composition (location of spectral features), the particle size (feature to continuum contrast), and the particle temperature (relative strength of short versus long wavelength features). The contribution from scattered light is not considered, as it is orders of magnitude weaker than dust emission in the mid-infrared (see our measurements of the system’s 0.8–35 μm SED shown in Figure 2(a)). The PSD is usually assumed to be a power law or power law reduced at small particle sizes to model radiation pressure blowout effects.

The list of materials tested included multiple amorphous silicates with olivine-like and pyroxene-like composition; multiple ferromagnesian silicates (forsterite, fayalite, clinopyroxene, orthopyroxene, augite, anorthite, bronzite, diopside, and ferrosilite); silicas, both amorphous and crystalline (obsidian, tektites, quartz, cristobalite, tridymite); phyllosilicates (such as saponite, serpentine, smectite, montmorillonite, and chlorite); sulfates (such as gypsum, ferrosulfate, and magnesium sulfate); oxides (including various aluminas, spinels, hibonite, magnetite, and hematite); Mg/Fe sulfides (including pyrothite, troilite, pyrite, and ningerite); carbonate minerals (including calcite, aragonite, dolomite, magnesite, and siderite); water–ice, clean and with carbon dioxide, carbon monoxide, methane, and ammonia clathrates; carbon dioxide ice; graphitic and amorphous carbon; and the neutral and ionized polycyclic aromatic hydrocarbon (PAH) emission models of Draine & Li (2007).

Our method has limited input assumptions, uses physically plausible laboratory emission measures from randomly oriented

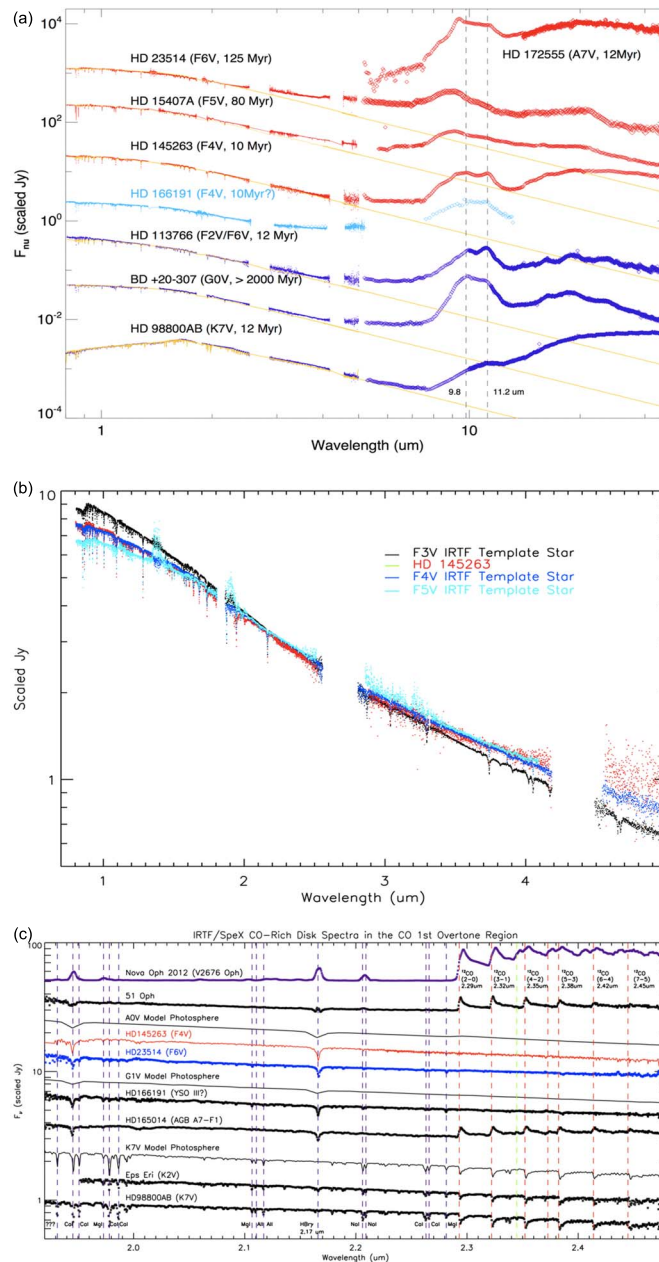


Figure 2. Panel (a): comparison of the 0.8–35 μm SpeX + 2009 IRS SED for HD 145263 to that of seven other warm dust systems (three silica dominated, in red; three silicate dominated, in dark blue; and one transition disk, in light blue). The MIR excesses of the silica systems have excess flux signatures extending to shorter wavelengths (7–9 μm) than the silicate disks (9–11 μm), as the silica SiO fundamental stretches are at 8–9 μm . The HD 172555 IRS spectrum at the upper right shows the strongest and most pronounced silica dust emission features. HD 23514 and HD 15407A show smooth excess emission features mainly dominated by silica dust; HD 113766 and BD+20-307 show the multiple peaked 8–13 μm structure typical of mixed olivine + pyroxene silicate dusts. HD 145263 is a hybrid mix between the two, evincing multiple 8–13 peaks as well as a pronounced 7–8 μm shoulder. Transition disk HD 166191, only observed using ground-based observations (Kennedy et al. 2014), looks very similar to HD 145263. HD 98800AB is silicate rich, but the MIR SED is dominated by a huge amount of $T \sim 150$ K long wavelength large dust particle blackbody emission seen as a minority contributor in HD 172555 and HD 145263. All seven of the IRS spectra show significant excess out to the 35 μm Spitzer/IRS cutoff, consistent with their being abundant dust particles with radii >30 μm present. Panel (b): HD 145263’s 1–4 μm spectral structure best matches that of an IRTF spectral library archival template star F4V star, quite different from previous descriptions of the star’s spectral type as F0V (Sylvester & Mannings 2000; Honda et al. 2004). Panel (c): detailed view of the HD 145263 IRTF/SpeX spectrum in the 1.9–2.4 μm wavelength range, showing the lack of CO, He I, Fe II, HBr γ , H $_2$ S(0), and S I/Sr I/Si I emission lines as seen in the spectra of other NIRDS targets, like NovaOph, 51Oph, and HD 166191. There are no spectral earmarks due to circumstellar gas in this system, nor is there any evidence of high-temperature processes like photospheric accretion, wind outflow, or dust sublimation. The Fe/Si and Mg/Si EW ratios are also similar to those for other early solar abundance F stars in our sample, ruling out unusual, non-solar abundance patterns producing the observed dust mineralogy. Panels (d) and (e): SpeX 0.96–1.07 and 1.48–1.75 μm absorption line spectra of HD 145263 vs. NIRDS spectra and “stellar template” (i.e., IRTF/SpeX on-line stellar library archival spectra) spectra of matching stellar type. Major clean (i.e., unconfused) atomic absorption lines are marked by vertical dashed lines in both plots. Panel (d) shows that HD 145263 primary’s absorption features are much more consistent with the deeper and more structured lines of the mid-F stars (e.g., at 0.988, 1.042, 1.068, and 1.083 μm) in our NIRDS sample than for the previous literature F0V assignment for the star. In panel (e), we show the HD 145263—F4V correspondence for the 1.49–1.75 μm range. HD 145263 has been matched to an F4V template star’s spectrum from the NASA/IRTF SpeX spectral library (red curve). Spectral comparisons for two other silica-dominated debris disk systems are also shown—HD 15407A has been matched to an F5V star’s spectrum (green curve), and HD 23514 has been matched to an F6V spectrum (blue curve) and a G0V star’s spectrum (aqua curve). In panels (d) and (e), there is no obvious difference between the spectra of silica disk hosting stars and the non-hosting template stars in this highly diagnostic spectral range, arguing against any unusual primordial system abundances causing the observed silica-rich dust.

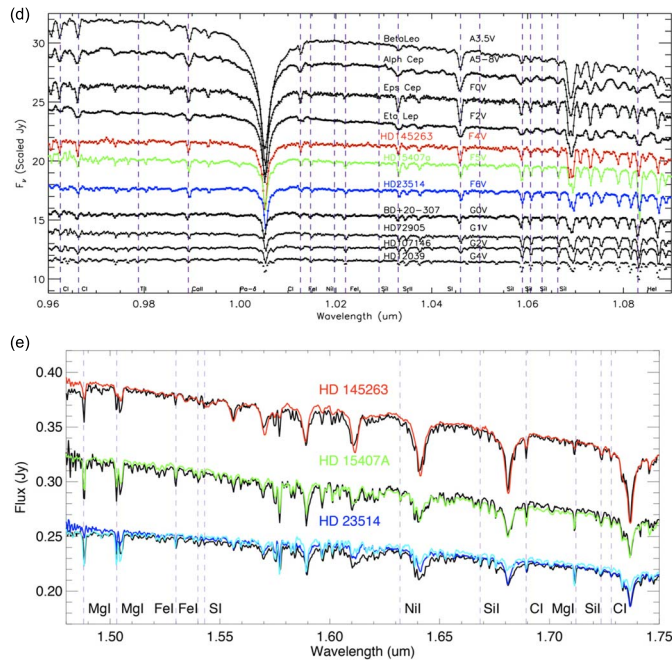


Figure 2. (Continued.)

powders rather than theoretically derived values from models of highly idealized dust, and simultaneously minimizes the number of adjustable parameters. The free parameters of the model are the relative abundance of each detected mineral species, the temperature of the smallest particle of each mineral species, and the PSD power-law slope (Table 3). The best fits are found by a direct search through (composition, temperature, PSD slope) phase space. Goodness-of-fit is determined using the reduced χ_ν^2 95% confidence limit for the number of spectral degrees of freedom in each spectrum. (For more details of our spectral modeling analysis, we refer the reader to the descriptions given in Lisse et al. 2006, 2007a, 2007b, 2008, 2009, 2012; Reach et al. 2010, and Sitko et al. 2011.)

In Figure 3, we show how, using our spectral modeling, we can analyze the Spitzer observations and derive a dust mineralogy. (We focus on the Spitzer data as the longer wavelength baseline is much more constraining for the mineralogical makeup of HD 145263’s circumstellar dust than the 8–13 μm Subaru/COMICS spectra, while the concordance of all five of the HD 145623 mid-infrared spectra shown in Figure 1(a) shows that the Spitzer spectra are good proxies for the Subaru epochs as well.) We also present the Spitzer/IRS HD 172555 debris disk spectrum, in order to show how markedly qualitatively different it is in the sharpness of its emission peaks (due to ultrafine dust) and the lack of pyroxene features at 9.8 and 10.3 μm . et al. 2016). Figure 4 shows, in a graphical pie chart form, the relative abundance of each dust species during the three Spitzer epochs of 5–35 μm spectroscopy.

3.2. Mineralogical Modeling Results

Model phase-space searching easily ruled out the presence of a vast majority of our library mineral species from the HD 145263 disk. Convincing evidence was found only for the following majority species in the 2005–2009 Spitzer spectra (Table 3, Figure 3): crystalline silicate forsterite, ferrosilite; amorphous silicates with pyroxene-like composition and a tiny

amount of olivine-like composition; large amounts of tektite-like hydrated silica; and amorphous carbon. The forsterite, amorphous carbon, and dominant ($M = 10^{22}$ – 10^{23} kg), cold ($T \sim 150$ K), optically thick rubble was found to be about the same at all epochs. After searching through phase space for the best-fit PSD power-law index, a single power law of $dn/da \sim a^{-3.75}$ was found to fit all of the Spitzer epochs well. Thus, a size distribution of fine dust similar to that found for the more active solar system comets was found to produce the strong mid-infrared spectral features seen, and the mass of this dust was roughly constant throughout.

The results of our mid-infrared spectral modeling of the three 2005–2009 HD 145263 Spitzer/IRS 5–35 μm spectra are shown in Figures 3 and 4 and are listed in Tables 3 and 4. In each case, we find dominant amorphous silica and amorphous pyroxene components, with about the same amount of amorphous carbon and crystalline Mg-olivine as in 2003. Very interestingly, all of the Fe-olivine fayalite, FeMgS_x , orthoenstatite, diopside, and water ice typically found in primitive cometary dust spectra (and by extension PPD disk dust; Bregman et al. 1987; Herter et al. 1987; Lisse et al. 2006, 2007a; Reach et al. 2010; Sitko et al. 2011) are missing from these spectra, as is two-thirds of the amorphous olivine, while large reservoirs of amorphous pyroxene and silica are present, along with some ferrosilite, to make a dust population quite unlike any we have ever studied before (including HD 172555, Figure 3(d)). The relative amount of forsterite, amorphous carbon, and silica found from 2005 to 2009 seems steady within the ± 0.02 (2σ) noise of the spectral decomposition measurement, while there does seem to be a slight upward trend of amorphous silicate of olivine composition coupled with a slight downward trend of amorphous silicate of pyroxene composition.

A strong signature of “SiO gas” is also present. However, since Lisse et al. (2009), studies by Johnson et al. (2012) and Wilson et al. (2016) cast some doubt on the presence of this

Table 3
Composition of the Best-fit Models^a for the 2005, 2007, 2009 HD 145263 Spitzer Spectra

Species	Density (g cm ⁻³)	Molecular Weight	Comet ^b Dust	HD 145263 2005	Weighted 2007	Surface Area ^c 2009	Model ^d T _{max} (K)	Model χ^2_ν if Species not Included
<u>Detections</u>								
<u>Olivines</u>								
AmorphSil/Olivine Composition (MgFeSiO ₄)	3.6	172	0.38	0.04	0.12	0.11	350	24.0/0.88/4.00/3.77
Forsterite (Mg ₂ SiO ₄)	3.2	140	0.23	0.26	0.23	0.22	350	1.91/1.88/2.49/2.49
<u>Pyroxenes</u>								
AmorphSil/Pyroxene Composition (MgFeSi ₂ O ₆)	3.5	232	0.06	0.42	0.31	0.28	350	1.63/20.5/16.6/15.4
FerroSilite (Fe ₂ Si ₂ O ₆)	4.0	264	0.00	0.14	0.04	0.11	350	0.84/1.50/1.04/1.73
<u>Organics</u>								
Amorph Carbon (C)	2.5	12	0.28	0.28	0.24	0.23	500	16.1/1.94/2.29/2.20
<u>Silicas</u>								
Tektite (Bediasite) (66% SiO ₂ , 14% Al ₂ O ₃ , 7% MgO, 6% CaO, 4% FeO, 2% K ₂ O, 1.5% Na ₂ O) ^e	2.6	62	0.00	0.31	0.37	0.31	350	0.84/8.45/16.1/12.7
SiO Gas (100% SiO)	N/A	44	0.00	0.34	0.38	0.35	350	0.84/1.87/2.90/2.71
<u>Upper Limits and Non-Detections</u> ^f								
<u>Silicas and Silicates</u>								
Amorphous Silica	2.7	60	0.02	0.00	0.00	0.00	350	0.84/0.67/0.93/0.93
Quartz	2.65	60	0.00	0.00	0.00	0.00	350	0.84/0.67/0.93/0.93
Ortho-Pyroxene (Mg ₂ Si ₂ O ₆)	3.2	200	0.11	0.00	0.00	0.02	350	1.39/0.67/0.93/0.99
Ortho-Pyroxene (Mg ₂ Si ₂ O ₆)	3.2	200	0.11	0.00	0.00	0.02	350	1.39/0.67/0.93/0.99
Diopside (CaMgSi ₂ O ₆)	3.3	216	0.14	0.00	0.00	0.00	350	1.23/0.67/0.93/0.93
<u>Metal Sulfides</u>								
Ningerite (as Mg _{0.10} Fe _{0.90} S)	4.5	84	0.10	0.00	0.00	0.00	350	3.78/0.00/0.00/0.00
<u>Water</u>								
Water Gas (H ₂ O)	1.0	18	0.08	0.00	0.00	0.00	210	0.87/0.67/0.93/0.93
Water Ice (H ₂ O)	1.0	18	0.22	0.00	0.00	0.00	210	16.2/0.67/0.93/0.93
<u>Phyllosilicates</u>								
Smectite (Nontronite) Na _{0.33} Fe ₂ (Si,Al) ₄ O ₁₀ (OH) ₂ * 3H ₂ O	2.3	496	0.00	0.00	0.01	0.00	350	0.84/0.67/0.97/0.93
Talc (Mg ₃ Si ₄ O ₁₀ (OH) ₂)	2.8	379	0.00	0.00	0.00	0.00	350	0.84/0.67/0.93/0.93
Saponite	2.3	480	0.01	0.00	0.00	0.00	350	0.87/0.67/0.93/0.93
<u>Carbonates</u>								
Magnesite (MgCO ₃)	3.1	84	0.02	0.00	0.00	0.00	350	0.88/0.67/0.93/0.93
Siderite (FeCO ₃)	3.9	116	0.02	0.00	0.00	0.00	350	0.88/0.67/0.93/0.93
<u>Oxides</u>								
Magnetite (Fe ₃ O ₄)	5.2	232	0.00	0.00	0.00	0.04	350	0.84/0.67/0.93/1.45

Notes.

^a Best-fit χ^2_ν model with power-law particle size distribution $dn/da \sim a^{-3.75}$, range of fit = 8–13 μm (2003), 6.3–34.7 μm (2005–2009). 95% C.L. has $\chi^2_\nu = 1.01/0.85/1.10/1.10$.

^b Comet dust mineralogical composition as determined for the very primitive material of comet 73P/Schwassmann–Wachmann 3 as measured by Spitzer (Sitko et al. 2011).

^c Weight of the emissivity spectrum of each dust species required to match the HD 145263 emissivity spectrum, including a large rubble BB fit. Uncertainties on these are typically 0.02 (2 σ), and weighted surface areas of any species at the ≤ 0.02 level are treated as non-detections.

^d All temperatures are ± 10 K (1 σ). $T_{\text{LTE}} @ r_h = 3.0$ au from the 4.1 L_{solar} HD 145263 primary ~ 285 K. The best-fit temperature for the largest rubble grains, which act like a long wavelength cold blackbody function addition to the 5–15 μm portion of the spectrum, has $T_{\text{bb}} = 150$ K, and amplitude = 2.1/0.9/0.9 in 2005/2007/2009.

^e Koeberl (1988).

^f Upper Limits and Non-Detections: species that appear to improve the fit by eye but do not improve the χ^2_ν value above the 95% C.L. limit. These include crystalline silica, water, phyllosilicates, carbonates, and iron oxides, all expected products of aqueous alteration of rocky dust.

species, both from a photolytic stability and an actual measurement standpoint. The amorphous silicates/silica study of Speck et al. (2011), and the Mars Spirit rover study of Ruff et al. (2011) have demonstrated that this 8 μm shoulder feature may be a solid-state feature found in hydrated forms of silica like hyalite (but not unhydrated forms like obsidian, cristobalite, or tektite). Our own 70+ IRTF/Spex survey results of

warm debris disks (Figure 2) did not find any 4–5 μm SiO overtone emission in the three silica disk systems studied, including HD 145263. Importantly, the amplitude of the SiO gas feature is just as strong as the unhydrated tektite silica in each of our fits. We thus consider, at this point, that the “SiO gas feature” could be describing a hydrated silica solid-state absorption feature and could just as well be telling us about the

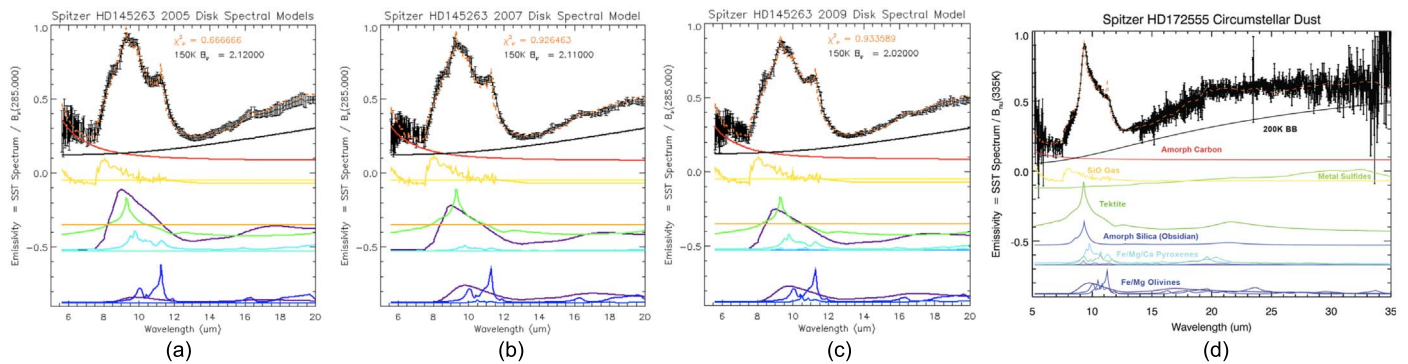


Figure 3. Mineralogical model decompositions of the Spitzer spectra. Panels (a)–(c): three panels corresponding to the three 2005–2009 epochs of Spitzer spectral observation of HD 145263. At the top of each panel in black are the temperature-independent “emissivity spectra” (i.e., observed flux vs. wavelength divided by a simple best-fit blackbody). The dashed orange line is our best-fit laboratory analog emissivity model. Error bars are 2σ . Informed by our previous model fits to cometary, asteroidal, and debris disk spectra (Lisse et al. 2006, 2007a, 2007b, 2008, 2009, 2012; Reach et al. 2010; Currie et al. 2011; Sitko et al. 2011), we tried linear combinations of 80+ different materials to see how well they would match the observed emissivity. The results quickly boiled down to a simple, refractory mixture of amorphous pyroxene (middle dark purple), amorphous carbon (red), amorphous silica (bright green), SiO gas/hydrated silica (yellow), crystalline olivine (forsterite, dark blue), and amorphous olivine (lower dark purple) and crystalline pyroxene (ferrosilite, light blue). The amplitude of each colored curve denotes its relative abundance in the fit; for example, the dark purple amorphous pyroxene abundance is $\sim 2\times$ more abundant in 2005 than it is in 2009. The same basic recipe fit all three epochs of Spitzer spectra (orange dashed curve), with relatively more amorphous pyroxene and carbon in 2005 and more amorphous olivine in 2009. Of greatest importance is the mineralogy: the 2005–2009 dust populations contain no crystalline Fe-olivine fayalite, Fe sulfides, crystalline pyroxene orthoenstatite or diopside or water ice, and very little amorphous olivine, while large reservoirs of amorphous pyroxene and silica are present, along with some ferrosilite, very different from any primitive dust mineralogy we have ever studied. Panel (d): reproduction of our best-fit spectral decomposition model from our 2009 HD 172555 study (Lisse et al. 2009; Johnson et al. 2012), with the color coding of the observations and individual components the same as in panels (a)–(c). This debris disk is overwhelmingly dominated by very fine silica dust, without any obvious amorphous pyroxene, and the minor silicate components are both Mg- and Fe-rich. Ferromagnesian metal sulfides are also present. The chemistry of this dust is very different than that of the HD 145263 disk dust.

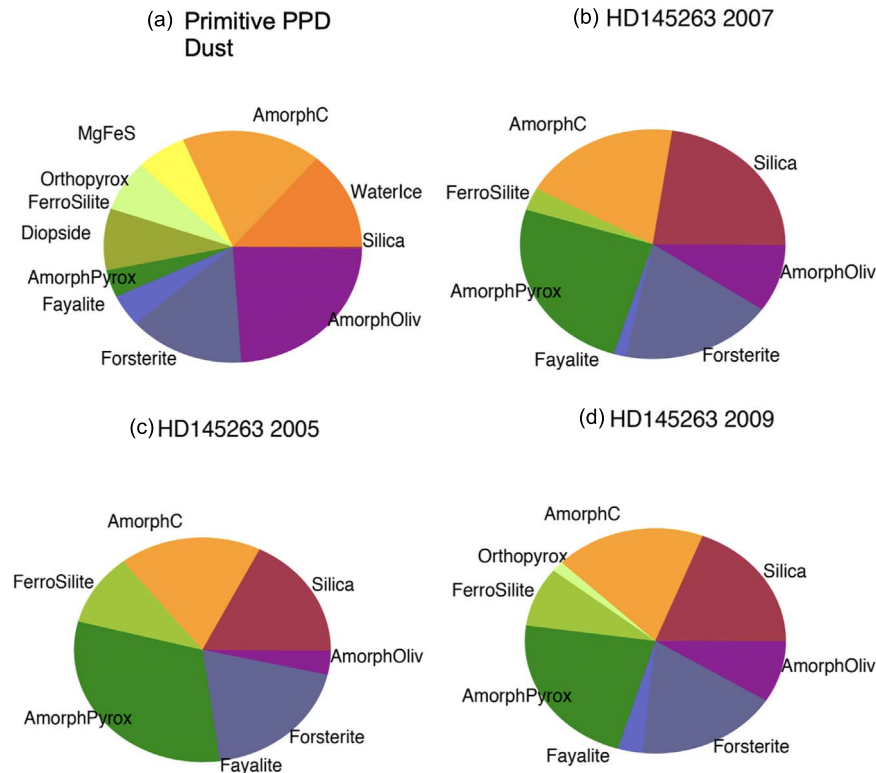


Figure 4. Pie charts showing the relative surface areas of the minerals detected in the circumstellar dust of HD 145263. Panel (a): relative surface areas of the dust mineral components in a PPD system, as estimated using a comet-like mineralogy with no silica + abundant water ice, FeMg-sulfides and an amorphous/crystalline mix of FeMg olivines and pyroxenes (Lisse et al. 2006, 2007a, 2007b). Panels (b)–(d): the markedly different mineralogical mixes of 2005–2009: Fe-olivine, FeMgS, and water ice are absent, while silica and amorphous pyroxene are superabundant. Crystalline Mg-olivine and amorphous carbon are found at levels expected for primitive cometary dust. The dust mineralogical mix is relatively stable from 2005 to 2009.

amount of hydration of any silica present as it is about the presence of SiO gas in a system.

In Table 4, we present the derived atomic abundance counts in the detected disk dust versus that from a mix of comet-like

dust. The H, C, O, Mg, Fe, S, and Ca abundances versus Si are markedly lower in the Spitzer spectra relative to those found in comet-like dust, as expected for mechanisms involving evaporation of low-temperature volatiles and sputtering of

Table 4
HD 145263 Circumstellar Dust vs. Cometary Dust Molar Atomic Abundances^a

Species	Best-fit Models	Relative to Si = 1.0	Relative to Solar ^b
	Comet/2005/2007/2009	Comet/2005/2007/2009	Comet/2005/2007/2009
H	0.024/0.00/0.00/0.00	1.01/0.00/0.00/0.00	3.2e-5/0.00/0.00/0.00
C	0.058/0.05/0.05/0.048	2.40/1.64/1.64/1.57	0.32/0.22/0.22/0.21
O	0.100/0.096/0.096/0.10	4.11/3.1/3.1/3.3	0.17/0.13/0.13/0.14
Si	0.024/0.03/0.03/0.03	1.00/1.00/1.00/1.00	1.00/1.00/1.00/1.00
Mg	0.026/0.018/0.018/0.017	1.05/0.58/0.58/0.57	1.00/0.56/0.56/0.54
Fe	0.017/9.9e-3/9.9e-3/0.015	0.68/0.32/0.32/0.48	0.79/0.37/0.37/0.56
S	0.0053/0.00/0.00/0.00	0.22/0.00/0.00/0.00	0.51/0.00/0.00/0.00
Ca	0.0021/9.6e-5/9.6e-5/8.1e-5	0.088/3.2e-3/3.2e-3/2.6e-3	1.40/0.050/0.050/0.42
Al	0.000/4.3e-3/4.3e-3/3.6e-3	0.000/0.14/0.14/0.12	0.000/1.98/1.98/1.66
Na	0.000/0.00047/0.00047/0.00039	0.000/0.015/0.015/0.013	0.000/??/?/?/??/?/?

Notes.

^a Molecular $N_{\text{moles}}(i) \sim \text{Density}(i)/\text{Molecular Weight}(i) * \text{Weighted Surface Area}(i)$ values given in Table 3, and atomic models are derived by summing up the atoms contained in each mineral species. Errors are $\pm 10\%$ (1σ).

^b Assuming the solar atomic abundances values versus Si are 3^o:1^o:104: 7.6:14.1:1.00:1.05:0.87:0.43:0.063:0.072 (Anders & Grevesse 1989; Asplund et al. 2005).

rocky materials by stellar wind energetic particles. Al and Na, which are more volatile rock-forming elements than Ca, are slightly higher in abundance in the 2005–2009 Spitzer spectra relative to comet-like dust.

4. Discussion

The goal of this paper is to use the information at hand to determine what could have formed the abundant silica found orbiting around HD 145263. Some quick conclusions can be made: In addition to the five epochs of mid-infrared spectral observations already presented, the sixth epoch includes an 0.8–5.0 μm IRTF/SpeX medium-resolution spectrum to work with (Figure 2), which immediately shows us that there is no detectable CO or H₂O circumstellar gas in the system, so that flash heating by nebular shocks are unlikely; a much more sensitive search with ALMA for CO has also been negative (Liemann-Sifry et al. 2016). The IRTF/SpeX data also show that the Fe/Mg/Si stellar abundance ratios look normal and solar, so collisional grinding of silica-rich planetesimals is unlikely operant mechanisms for silica dust creation. (If the HD 145263 system was somehow extremely Si-rich compared to solar, we could possibly expect a felsic dust composition containing predominantly silica + feldspars.) Because the dust temperature we derive from the SpeX + IRS SEDs (Figures 2, 5) is a moderate ~ 285 K, far below the ferromagnesian silicate melting temperature of ~ 1000 K, and because we find no detectable atomic sublimation emission features in our 2011 HD 145263 SpeX spectrum (like we saw for HR4796A, Lisse et al. 2017b), we can rule out close-in β Meteoroid formation via dust-grain sublimation as a silica source.

Instead, we focus on large-scale stochastic processes such as stellar flares (Osten & Wolk 2015) or giant impacts (Lisse et al. 2009) in HD 145263’s past. We also need to consider that any debris disk in apparent steady state must be producing new dust to offset the removal of dust by radiation and stellar wind pressure and Poynting–Robertson drag, and that these sources have to be large, as the overall sensible surface area of the disk is on the order of 10 times that of the 10²² kg HD 172555 disk. So, unless the removal processes are very slow, whatever

altered the orbiting dust population also seems to have altered its sourcing planetesimals.

This leads us to the following hypotheses for the production of silica in HD 145263’s disk: (1) a giant impact involving large comet-like planetesimals destroyed all of their highly volatile ices and metal sulfides, while reforming their less refractory rocky components into silica materials. (2) Visible light from a megascale stellar-flare thermally flash-vaporized and re-processed all of the orbiting dust and the surfaces of all sourcing grinding planetesimals. (3) A large stellar-flare input enough energy to cause severe space weathering via low-temperature heating + stellar wind sputtering of the surface layers of the circumstellar dust + sourcing grinding planetesimals.

Each of these hypotheses has pros and cons versus the known data for the system, as we lay out next. With the current data, we currently favor Hypothesis (3) and find fatal flaws with Hypotheses (1) and (2).

Before we go into detailed discussion of each of these model scenarios in turn, we compare in Table 5 what we know about the system’s circumstellar dust properties versus other characterized disks. We see that it has some of the largest amounts (M_{Moon} to M_{Mars}) of sensible warm, ~ 300 K dust found in any non-primordial circumstellar disk. Given the system’s young ~ 11 Myr old age and lack of circumstellar gas, the high disk mass is consistent with a transition disk system that is building planets or has just finished building planets (like HD 11376 or HD 166191; Kenyon & Bromley 2006, 2016; Lisse et al. 2008; Kennedy et al. 2014; Genda et al. 2016). We also note that compared to the circumstellar dust in other young, primitive, silicate-rich debris disks, Mg-olivine and amorphous carbon components are present at expected roughly comet/PPD levels, while amorphous and Fe-crystalline olivine have disappeared, apparently replaced instead with super-abundant amorphous pyroxene and silica. The O:Si, C:Si, Mg:Si, and Fe:Si ratios are all lower than expected for primitive cometary material, showing evidence for selective O and Fe atom removal (Tables 3 and 4). This additional information will be important for discussing and evaluating the following

Table 5
Derived Total Masses for Selected Relevant ExoDisks and Solar System Objects

Object	Observer Distance (1) (pc au ⁻¹)	Mean Temp (2) (K)	Equivalent Radius (3) (km)	19 μm Flux (4) (Jy)	Approximate Mass (5) (kg)
Earth	...	282	6380		6×10^{24}
Mars	1.5 au	228	3400		6×10^{23}
HD 113766 (F2/F6)	109 pc	440	≥ 2700 (270)	1.85	$\geq 2.3 \times 10^{23}$ (5.3×10^{20})
HD 145263/2005-9 (F4)	142 pc	285	≥ 2180 (1150)	0.49	$> 1.8 \times 10^{23}$ (3.5×10^{21})
ID8 (G8)	357 pc	900	≥ 2300 (520)	0.011	$\geq 1.4 \times 10^{23}$ (1.4×10^{21})
Moon	0.0026 au	282	1740		7×10^{22}
η Corvi (F2) Cold Dust	18 pc	~35	≥ 1600		$\geq 6 \times 10^{22}$
KBO Pluto	40 au	45	1190		1.3×10^{22}
HD 172555 (A5)	29 pc	335	≥ 910 (250)	0.90	$> 10^{22}$ (1×10^{20})
HD 100546 (Be9V)	103.4 pc	250/135	≥ 910	203	$\geq 1 \times 10^{22}$
Asteroid Belt	0.1–5.0 au	Variable	577		3×10^{21}
Asteroid	0.1–5.0 au	Variable	1–470		1×10^{13} – 9×10^{20}
KBO Orcus	30–45 au	42–52	300		6×10^{20}
Earth’s Oceans	...	282	300		6×10^{20}
Enceladus	10.5 au	75–135 K	252		1×10^{20}
Miranda	19.2 au	~65	235		7×10^{19}
η Corvi (F2) Warm Dust	18.2 pc	400	≥ 900 (140)		$\geq 9 \times 10^{21}$ (9×10^{18})
KBO 1996 TO66	38–48 au	41–46	~200		$\sim 4 \times 10^{19}$
Centaur Chiron	9–19 au	65–95	~120		$\sim 1 \times 10^{19}$
Outer Zody Cloud	5–100 au	25–100	84		4.9×10^{18}
HD 69830 (K0V)	12.6 pc	340	≥ 60 (30)	0.11	$\geq 2 \times 10^{18}$ (3×10^{17})
Inner Zody Cloud	0.1–5.0 au	260	9–14		1 – 4×10^{16}
Comet nucleus	0.1–10 au	Variable	0.1–30		10^{12} – 10^{15}
Hale–Bopp coma	3.0 au	200		144	2×10^9
Tempel 1 ejecta	1.51 au	340		3.8	1×10^6

Notes. (1)—Distance from Observer to Object, updated for *Gaia* DR2 measurements (Bailer-Jones et al. 2018). (2)—Mean temperature of thermally emitting surface. (3)—Equivalent radius of solid body of 2.5 g cm^{-3} . (4)—System or disk averaged flux. (5)—Lower limits are conservative, assuming dust particles of size of 0.1–100 μm (as detected by Spitzer, in parentheses), or 0.1 μm–100 m (extrapolated using the best-fit power-law PSD), ignoring optical thickness effects. For HD 172555, we have included the mass of SiO gas and large particle rubble in the estimate. For η Corvi, we quote the directly observed (by remote sensing) 0.1–100 μm mass in the abstract and use this quantity for determination of the minimum mass delivered.

heat the dust to boiling temperatures. Such a flare should be easily detectable from the Earth—and some are. According to Davenport (2016) and Van Doorselaere et al. (2017)’s flare studies of Kepler/K2 stars, about 1.6% of such young F stars flare detectably in the optical, but they can super-flare with energies up to 3×10^{31} J. These super-flares are very brief, on the order of 1–2 hr in duration, and occur every 10^4 – 10^5 days, so one of them could easily be missed by AAVSO-like variable star surveys observing on timescales of days to weeks.

In this scenario, HD 145263’s circumstellar-disk material was transformed on very short timescales of hours (10^4 – 10^5 s) sometime pre-2001 (the start of the ASAS monitoring of the system, Section 2.1), with melting and vaporization to significant depth accompanied by a huge impulse in radiation pressure. SiO gas was naturally formed via fast vaporization of silicate dust, and silicas by quick re-freezing of the vapor. Removal of all pre-existing sub-blowout-sized dust occurred, combined with a new PSD created by equilibrium recondensation and subsequent collisional grinding.

While this mechanism can explain the collisional-equilibrium like PSD, we find for HD 145263’s disk dust from the Spitzer IRS spectra (Section 3), a major discrepancy between the predictions of this mechanism for HD 145263’s dust disk transformation and the observations are the presence of low melting point pyroxenes and the absence of crystalline

Fe-olivine in HD 145263’s disk dust (Figures 4 and 5). This combination of materials does not agree with the predicted thermal destruction of the least refractory ice, metal sulfide, and pyroxene species typically found in primitive PPD dust.

A variant on the giant stellar-flare theme of note is a giant stellar flare induced by a giant impact onto the primary star. As has been suggested by the recent work of Brown (2011, 2015) in studying the sungrazing comet phenomenon in our solar system, a comet coming to perihelion in the Sun’s photosphere moves with a velocity $\sim 600 \text{ km s}^{-1}$ with respect to the Sun, so that even a medium-sized comet of $\sim 10^{13}$ kg can deliver on the order of 4×10^{24} J to the Sun upon impact. A medium-sized asteroid or KBO massing 10^{18} kg or more could easily deliver $\sim 10^{30}$ J to the HD 145263 primary’s photosphere. What happens after that is pure conjecture; we do know from FU Ori stars that violent energy outbursts with short rise times seem to accompany massive accretion events, although settling times are usually much longer than 1–2 yr and leave behind a tell-tale residual disk and its spectral signatures (Hartmann & Kenyon 1996; Green et al. 2006, 2016; Hubbard 2017). Singleton accretion events such as we are describing should happen most often in transition systems that have lost their primordial disks but have yet to clean out their planetesimal populations, and the low age of ~ 11 Myr for HD 145263 suggest that this could be plausible, although flares of this magnitude have yet to be observed in ~ 10 Myr old stars.

4.3. Space Weathering

Another variant on the stellar-flare scenario of Section 4.2 that preserves collisional-equilibrium particle shape, occurs at lower temperatures, requires much less energy, and acts selectively on Fe-silicates is the processing of circumstellar dust by stellar XUV and high-energy particles to alter the surface layers of the circumstellar dust down to a few mid-IR skin depths, deeper than $\sim 30 \mu\text{m}$. This can be done slowly, over millions of years, as in the exposed hard surfaces of bodies in our solar system, or more rapidly in the event of very large flaring events containing a similar equivalent total energy dose. If done quickly, the sputtering effects of stellar XUV and high-energy particles can combine with thermal effects to efficiently transform the surface layers of a rocky object, mainly by removing oxygen from the tetrasilicate lattice and producing nanophase Fe from $\text{Fe}^{+2/+3}$ counterions.

How does this scenario match up to what was observed in HD 145263? The observed mineralogical mix does not match up with any known spontaneous terrestrial chemical alteration of primitive cometary rocky material, nor the species found in aqueously altered asteroids. Aqueous alteration of silicates would *oxidize* the Fe^{+2} in the silicates, producing olivine and silica from pyroxene, along with phyllosilicates, carbonates, and Fe-oxides. We see none of the latter three materials in the Spitzer IRS mineralogy. This rules out the possibility of alteration to silica within compact bodies that this dust may have been sourced from. Flash vaporization and re-condensation of rocky material would create a mixture of high-temperature stable and kinetically favored products, i.e., olivines + silicas, as we saw in the HD 172555 disk system mineralogy, where pyroxenes had been almost totally destroyed (Figure 4). Since we do see abundant Fe-pyroxenes in the HD 145263 disk dust (Table 3), we can rule out a hypervelocity impact formation process for the dust. Instead, in HD 145263, the silicates have been *reduced* from a predominantly olivine composition to a predominantly pyroxene + silica composition, although Mg-olivine (forsterite) apparently remains unaltered.

This observed pattern of mineralogical change *is* consistent with low-level heating of primitive, mostly amorphous material. Temperatures would have to have been high enough to completely vaporize water ice and metal sulfides, while creating an appreciable vapor pressure of recondensing SiO. At the same time, temperatures would have to have stayed low enough to not alter the Mg olivines, implying $T < 1300 \text{ K}$ (Nuth & Johnson 2006). Depletion of O, C, Mg, and Fe could have occurred via this mechanism, as O, Mg, and Fe become volatile above 1000 C in tetrasilicates and the released O can attack the refractory C component, producing volatile CO and removing some of the C from the system. (One has to be careful about estimating the total system Fe, Mg, and O abundances because, while our NIR spectral allow us to rule out the presence of any appreciable circumstellar Fe/Mg atoms or low ionization state ions, there could be significant amounts of these atoms in hard to detect recondensed Fe- and Mg-oxides.) Sputtering alteration of the dust by energetic particles in HD 145263’s stellar wind could also play a role, with Fe-olivines again most easily reductively transformed in their optical properties (Quadery et al. 2015).

Moderate heating + energetic particle sputtering of dust in vacuum goes by another name in planetary astronomy—“space weathering,” and is a keen area of study for interpreting the

different surface reflectance spectra of the $\sim 10^6$ asteroids in our solar system (Reddy et al. 2012; Domingue et al. 2014; Kohout et al. 2014, 2016; Quadery et al. 2015; Schelling et al. 2015; Pieters & Noble 2016; Fazio et al. 2018). These studies generally show that of the common ferromagnesian tetrasilicates, it is easiest to weather Fe-bearing olivines into amorphous pyroxenes, silica, and Fe-metal via removal of Fe and O from the surface layers of the olivine. A critical point to add is that the amount of energy required to space-weather alter the optical properties of primitive-era HD 145263 circumstellar dust to appear like the present-era material to a few skin depths ($\sim 30 \mu\text{m}$) can be much lower than that required to totally vaporize and reform it, especially for the biggest dust grains. Assuming the net reaction is something like $8\text{H} + 3 \text{FeSiO}_4 \rightarrow \text{Fe}_2\text{SiO}_6 + 4 \text{Fe} + \text{SiO}_2 + 4 \text{H}_2\text{O}$, the total change in Gibbs free energy is $(-267.2 - 204.6 - 4 * 54.64 + 3 * 329.6) * 4.184 = +1250 \text{ kJ}/(3 \text{ moles of transformed fayalite})$, or $\sim 2.1 \text{ MJ kg}^{-1}$ of transformed fayalite (assuming 5 mol of fayalite/kg of rock). This is 15–25 times less energy/kg than the giant flare dust vaporization scenario of Section 4.2 requires, since the “low-level” heating to 1100–1300 K and stellar wind sputtering does not require bulk destructive vaporization of all of the circumstellar dust. If we further constrain the transformation to depths of $\sim 30 \mu\text{m}$, only about 5% of the $dn/da \sim a^{-3.75}$ (Section 3) dust mass needs to be space-weather altered, and the total flare energy required is reduced by a factor of 300–500 versus the 10^{29} – 10^{30} J we estimated in Section 4.1 required to vaporize the dust in place; i.e., we estimate that a total energy on the order of 10^{26} – 10^{27} J is sufficient to transform HD 145263’s dust from its primordial state to its present state. This is comfortably within the range of the larger stellar XUV flares seen in the Milky Way (Byrne 1989).

There is no listed X-ray detection or information about HD 145263’s X-ray luminosity in the archival literature; it was not detected in the *ROSAT* All-Sky Survey (RASS). We gain some assurance that an ~ 12 Myr old F4V star like HD 145263 should be XUV and stellar wind active using the Chandra values of $L_x = 2 \times 10^{21} \text{ W}$ for ~ 12 Myr old F2V star HD 113766A and $L_x = 2 \times 10^{22} \text{ W}$ for ~ 12 Myr old F6V star HD 113766B at $d \sim 120 \text{ pc}$ (Lisse et al. 2017a), and by noting that stellar X-ray emission and flaring activity increases markedly as one goes from early to late F-type stars. (A rotational period of 1.7 days for the HD 145263 primary (Section 2) implies a Rossby number of ~ 0.07 (Wright et al. 2011), and a star rotating rapidly versus its convective timescale in the $L_x = 0.0006 L_{\text{bol}}$ saturation regime. Using $L_x = 0.0006 L_{\text{bol}}$, we would estimate an even higher $L_x = 3 \times 10^{23} \text{ W}$.) Assuming that it is active, we can make an educated guess at its level of X-ray activity (or that of any nearby optically undetected M-type companions) using the RASS limiting sensitivity of $\sim 3 \times 10^{22} \text{ W}$ at $d = 142 \text{ pc}$. Since brief giant flares of up to $1000\times$ the quiescent emission level are not uncommon for young stars (Lammer et al. 2003; Ribas 2005; Guinan & Engle 2007; Osten & Wolk 2015), we can assume a most optimistic HD 145263 case with a giant XUV flare energy flux of $\sim 3 \times 10^{25} \text{ W}$, some three orders of magnitude lower than the maximal optical flare flux presented in Section 4.1. It would take 3×10^4 to $3 \times 10^6 \text{ s}$ (or 10 hr to 1 month, with the latter, longer estimate assuming that $\sim 5\%$ of the radiated XUV energy is directed into the disk and not into 4π of free space), to accumulate the $\sim 10^{27}$ J of XUV energy observed in the largest stellar magnetospheric flares/CMEs ever recorded (Byrne 1989; by contrast, the largest flare/CME total energy ever observed

from the modern, 4.56 Gyr old Sun is $\sim 10^{26}$ J in the Carrington event of 1856 and the great storm of 2012). A series of closely spaced (in time) flares could also produce the observed result, as long as the time required to achieve the total flare energy dosage is short compared to any patina removal timescales, which are on the order of decades (see Section 4.4).

Thus, an XUV flare irradiation mechanism could produce the olivine \rightarrow pyroxene + silica mineralogical transformation seen in HD 145263’s disk, while providing enough energy to transform an optically thick surface patina on the disk’s dust. From all of the evidence, then, the best explanation for what has occurred in HD 145263 is that we have encountered a severe case of space-weathering alteration of a young debris disk. If so, then the findings we have from studies of space weathering in our solar system can be applied to HD 145263’s disk material—e.g., we can expect the dust to be optically reddened versus the usual grayish neutral colors of silicates, and for there to be abundant nanophase Fe present.

4.4. Summary and Need for XU/VIS/IR Monitoring of Silica Debris Disk Systems

In summary, the only physical mechanism we currently know of that could produce the observed HD 145263 silica-rich dust mineralogy from an initially primitive dust reservoir would be space weathering caused by an epoch of unusually intense stellar wind or a giant stellar/XUV outburst from the central star. Unfortunately for this hypothesis, however, HD 145263 is not a detected source in the second *ROSAT* All-Sky Survey catalog (Boller et al. 2016), which adds little credence to the “active young star transforming nearby circumstellar dust” by frequent flaring over time scenario. On the other hand, we do not expect the average young mid-F star at 142 pc from the Earth and *ROSAT*, with $\log L_x = 28.9\text{--}29.5$ to be detectable in the RASS (Panzer et al. 1999; Favata & Micela 2003; Suchkov et al. 2003; Schmitt & Liefke 2004) and the star appears to be rotating rapidly enough with a 1.7 days period (Figures 1(b)–(c)) to be XUV active (Section 4.2). Nor do the AAVSO or superWASP photometric time series for the star in the 2003–2009 timeframe, which show no excursions larger than ~ 0.2 mag in apparent brightness from the mean (Figures 1(b), (c)) help advise us. Again on the other hand, giant stellar XUV flares often do not have optical counterparts (E. Shkolnik 2018, private communication; E. Guinan 2019, private communication) and can be of very short duration and so missed by weekly monitoring photometry (Balona 2012).

Because we only rarely see silica-dominated debris disks, we are driven toward assuming extreme space weathering due to some sort of unusually strong stellar wind or a stochastic, quick super-flare in the system, but have no direct proof of this. A super-flare disk transformation mechanism should be testable by high-cadence optical and X-ray light-curve monitoring of the system. One of the near-future methods of doing this would be to examine the current optical time domain behavior of this star, like the 2 minute cadence TESS light-curve data (Ricker 2015) for flares. At apparent visual magnitude $V \sim 9$, HD 145263 is comfortably above the TESS limiting magnitude of $V \sim 12$, and any photometric variations due to flaring should be detectable. Another indirect test of the space-weathering hypothesis is to measure the mineralogy of the HD 145263 disk over time, to see if the surface patina of reduced pyroxenes + silica wears off over a relatively short (in geologic and orbital terms) amount of time, as opposed to the Myr

estimated to replace flash refrozen dust from a massive hypervelocity impact (Jackson & Wyatt 2012).

There is a useful additional calculation we can make regarding timescales here. Any newly space-weathered dust should start being depleted as soon as it is created by the forces acting most readily on the small circumstellar particles, radiation pressure and P – R drag. In a collisionally supported dust population, however, quickly removed small particles can always be replaced by grinding down of longer-lived bigger particles, as long as they are present and contain significant amounts of space-weathered material to be ground. As large particles for which an $\sim 30 \mu\text{m}$ skin of space-weathered material is only a small fraction of the mass begin to grind down, they will replenish the original comet-like dust composition. The breakpoint size is about 0.3 mm diameter, the size at which a 30 μm altered skin would account for more than half the mass of a particle. This suggests that the evinced disk composition should trend back toward the original cometary composition on a timescale that is roughly the collision time for 0.3 mm particles in the HD 145263 disk. The collision time is roughly $1/(n\sigma v_{\text{rel}})$, where n is the number density, σ is the collisional cross section, and v_{rel} is the relative velocity. If we assume a disk width/radius ratio of about 0.1, for a disk width of 0.3 au and all of the 10^{22} kg of sensible dust in 0.3 mm dust grains with a density of 3.0 g cm^{-3} (Tables 3, 5), then we have $n \sim 3 \times 10^7 \text{ m}^{-3}$. If we also assume that the relative collision velocity is about 10% of the orbital velocity, and the collisional cross section is the dust hard sphere cross section for 0.3 mm diameter spheres, then that gives us a lower-limit to the collision clearing timescale of about 10 yr, or about 2.5 dust orbits around the primary. Since we do not see any appreciable change in the Subaru/COMICS 8–13 μm spectral character of the dust from 2003 through 2014, we can presume the dust has survived at least the expected minimum amount of collisional grinding time. But it is very possible that in the 5 yr since the last COMICS observation that the evinced dust surface composition could have started going back toward its primitive composition and that future observations in the 2020s, e.g., with JWST, or with ground-based mid-IR spectrometers currently available, should show this. A collisional support timescale on the order of 10 yr also explains why space-weathering effects are so ephemeral versus geological and solar system evolutionary timescales—severely altered space-weathered surface material is not well supported by the large particle reservoir for very long.

Further monitoring of the HD 145263 system in the MIR and X-ray is thus clearly warranted, to see if it does indeed occasionally super-flare, and if its dust has only been altered in a 10s of microns surface patina. The same can be said for the HD 172555 system. In comparison to our new HD 145263 result, the high-temperature mineralogy and extremely fine-grain-dominated dust-grain $dn/da \sim a^{-4.1}$ PSD we see in the HD 172555 silica-rich disk today *could not* have been formed via relatively gentle, shape-preserving space weathering. The transformation at $T > 1300$ K (to destroy all pyroxenes, and flash freeze new silica) would have to have been quick and severe, requiring incredibly high power levels in any super-flare—potentially like one of the $\sim 10^{31}$ J optical super-flares described in Section 4.2.

The planet–planet hypervelocity collision scenario we promulgated for producing the abundant silica found in the HD 172555 disk (Lisse et al. 2009) was determined using a

process of elimination of all known mechanisms for its creation. It still seems highly likely as a probable cause of the rare silica-dominated debris disks, as they are found in young systems in their planet-building phase, and planets are thought to grow to their final sizes via giant collisions (Kokubo & Ida 1998; Kenyon & Bromley 2006; Kokubo & Genda 2010; Jackson & Wyatt 2012). But the existence of such high-intensity, short-duration stellar flares was not known until the Kepler/K2 stellar survey work of 2012–2017 (Davenport 2016 and Van Doorselaere et al. 2017), and the new TESS work in 2019 (Gunther et al. 2020). Even though young, ~ 20 Myr old A7V stars like HD 172555 are seen to super-flare orders of magnitude less often than FGK stars, we need to add this new possibility of an optical super-flare totaling some 10^{30} – 10^{31} J energy transforming a pre-existing primitive dense dust disk to the list of possible causes.

This new possibility should be tested by new high-cadence optical monitoring. If optical super-flares are found from the HD 145263 primary, it will show that there are possibly three ways to make a silica-rich debris disk (via optical super-flares, XUV space weathering, or giant impacts). This will have important implications for how the silica around 25% of T Tauri stars and the silica found in solar system meteorites was made (Sargent et al. 2006). We will not know for sure, though, unless a future super-flare is seen coupled with another MIR spectral silica transformation event.

5. Conclusions

In this paper, we have presented spectra and photometry of the HD 145263 debris disk system over the 2003–2014 timeframe. We find an F4V host star surrounded by a stable, massive 10^{22} – 10^{23} kg dust disk equivalent to the material found in a Moon- to Mars-sized body. No gas was found in the circumstellar disk, and the primary star was found to be rotating at a rapid rate, with an ~ 1.75 days period. The silica + pyroxene rich mineralogy of the dust disk is very unusual compared to the ferromagnesian silicates typically found in primordial and debris disks.

Using our previous study of the young HD 172555 silica-rich debris disk (Lisse et al. 2009) as a guide, we raise a number of possible silica formation scenarios for HD 145263. But unlike that study, we have additional information: the time series of mid-infrared spectra straddling the appearance of circumstellar silica dust and a medium-resolution near-infrared NASA IRTF/Spex spectrum that allows us to rule out any stellar accretion, strong wind outflow, or unusual system mineralogical abundances. The same spectra do not show any SiO emission features in the 4–5 μm first overtone region, supporting our new supposition that the 8 μm “SiO gas feature” is explainable instead as a hydrated silica solid-state feature. Another important clue is produced by our spectral modeling: if we take a typical protoplanetary dust disk mineralogical mix and delete the Fe-rich olivines, water ice, and metal sulfides, and replace them with amorphous and Fe-rich crystalline pyroxene and silica, we can reproduce the Spitzer spectra. Putting this all together, we find that the only mechanism we can propose that is energetically reasonable for reductively altering an orbiting dust population in place as seen in space weathering triggered by giant stellar-flare transformation of the Fe-silicate components of the original cometary dust population.

Conversely, re-examining the Lisse et al. (2009) HD 172555 observations, we find a very different circumstellar dust population in that system, one that is heavily dominated by

fine silica dust. The minor constituents contain abundant silicate and metal-sulfide crystalline materials but little amorphous components. The HD 172555 population looks like a thermally annealed dust disk to which a huge amount of new glassy silica dust has been added. So a giant hypervelocity impact in this system, as we proposed in 2009, still seems to be a viable option. The work discussed here has added the possibility of a giant optical stellar flare melting and vaporizing a pre-existing dust disk.



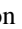




In sum, there may be up to three ways to make silica-rich debris disks, an idea consistent with the three qualitatively different kinds of silica disk MIR spectra seen in Figure 2(a) (HD 145263 + HD 166191; HD 172555; HD 23514 + HD 15407A) and that spectrally monitoring the known silica disks on yearly and decadal timescales would be useful to help discern the mechanism(s) of their production.

For HD 145263, with its space-weathered dust disk, we predict that there should be copious amounts of optically red, nanophase Fe-rich dust in the disk orbiting around the primary. We also predict that the space-weathering signature should disappear over time if the dust was truly altered only to a shallow 10s of microns depth, as the altered small particles are swept out of the system and grinding of larger particles to replace them exposes fresh, non-space-weathered dust. This should happen over collisional and radiative blowout timescales. It would then take another stochastic super-flare from the star to re-weather material and re-instate the silica + amorphous pyroxene appearance. It is thus important to obtain future high-cadence optical and X-ray light-curve monitoring of the system.

Finally, there is still the mystery of how 10^{22} – 10^{23} kg of dust became emplaced at ~ 3 au from the HD 145263’s F4V primary to begin with. The best explanation we can find is that the 10^{22} – 10^{23} kg of dust is some of the last remnants of the HD 145263 system’s original primordial disk and that we are seeing a transition disk’s processing (Section 2), but this needs to be proven by future work. This line of inquiry has important implications for the creation of silica found in abundance orbiting around $\sim 25\%$ of T Tauri stars and in some primitive solar system meteoritic materials (Sargent et al. 2006), and it needs to be pursued in order to better understand early solar system development.

This paper was based on observations taken with the NASA Spitzer Space Telescope, operated by JPL/Caltech, on observations taken by the Subaru Telescope, funded and supported by the National Astronomical Observatory of Japan, and on observations taken with the IRTF/Spex 0.8–5.5 Micron Medium-Resolution Spectrograph and Imager, funded by the National Science Foundation and NASA and operated by the NASA Infrared Telescope Facility. The authors would like to acknowledge help in obtaining the data from H. Fujiwara, M. Honda, and J. Rayner, and highly useful comments and suggestions received from colleagues S. Engle, E. Guinan, M. Perrin, and D. Watson used in forming the analysis and discussion presented in this paper. C.M.L. gratefully acknowledges support for performing the modeling described herein from JPL Spitzer contract 1274485, NASA NExSS grant to ASU NNX15AD53G, and NSF Grant AST-0908815. M.D.L. was supported by a scholarship from the NASA Iowa Space Grant Consortium.

ORCID iDs

C. M. Lisse  <https://orcid.org/0000-0002-9548-1526>
 H. Y. A. Meng  <https://orcid.org/0000-0003-0006-7937>
 M. L. Sitko  <https://orcid.org/0000-0003-1799-1755>
 B. C. Johnson  <https://orcid.org/0000-0002-4267-093X>
 A. P. Jackson  <https://orcid.org/0000-0003-4393-9520>
 R. J. Vervack, Jr.  <https://orcid.org/0000-0002-8227-9564>
 S. J. Wolk  <https://orcid.org/0000-0002-0826-9261>
 M. Marengo  <https://orcid.org/0000-0001-9910-9230>

References

- Anders, E., & Grevesse, N. 1989, *GeCoA*, **53**, 197
 Andrae, R., Fousneau, M., Creevey, O., et al. 2018, *A&A*, **616**, A8
 Asplund, M., Grevesse, N., & Sauval, A. J. 2005, in ASP Conf. Ser. 336, Cosmic Abundances as Records of Stellar Evolution and Nucleosynthesis, ed. F. N. Bash & T. G. Barnes (San Francisco: ASP), 25
 Bailer-Jones, C. A. L., Rybizki, J., Fousneau, M., Mantelet, G., & Andrae, R. 2018, *AJ*, **156**, 2
 Balona, L. A. 2012, *MNRAS*, **423**, 3420
 Boller, Th., Freyburg, M. J., & Truemper, J. 2016, *A&A*, **588**, A103
 Bregman, J. D., Witteborn, F. C., Allamandola, L. J., et al. 1987, *A&A*, **187**, 616
 Brown, J. C., Carlson, R. W., & Toner, M. P. 2015, *ApJ*, **807**, 165
 Brown, J. C., Potts, H. E., Porter, L. J., & Le Chat, G. 2011, *A&A*, **535**, A71
 Butters, O. W., West, R. G., Anderson, D. R., et al. 2010, *A&A*, **520**, L10
 Byrne, P. B. 1989, *SoPh*, **121**, 61
 Chambers, J. E. 2013, *Icar*, **224**, 43
 Chen, C. H., Mamajek, E. E., Bitner, M. A., et al. 2011, *ApJ*, **738**, 122
 Chen, C. H., Mittal, T., Kuchner, M., et al. 2014, *ApJS*, **211**, 25
 Currie, T., Lisse, C. M., Sicilia-Aguilar, A., et al. 2011, *ApJ*, **734**, 115
 Davenport, J. R. A. 2016, *ApJ*, **829**, 23
 Domingue, D. L., Chapman, C. R., Killen, R. M., et al. 2014, *SSRv*, **181**, 121
 Draine, B. T., & Li, A. 2007, *ApJ*, **657**, 810
 Engler, N., Schmid, H. M., Quanz, S. P., Avenhaus, H., & Bazzon, A. 2018, *A&A*, **618**, A151
 Faure, G. 1998, Principles and Applications of Geochemistry (2nd ed.; Upper Saddle River, NJ: Prentice Hall), <https://instruct.uwo.ca/earth-sci/300b-001/0910thermo.htm>
 Favata, F., & Micela, G. 2003, *SSRv*, **108**, 577
 Fazio, A., Harries, D., Matthäus, G., et al. 2018, *Icar*, **299**, 240
 Fedele, D., van den Ancker, M. E., Henning, T., Jayawardhana, R., & Oliveira, J. 2010, *A&A*, **510**, 72
 Fujiwara, H., Ishihara, D., Onaka, T., et al. 2013, *A&A*, **550**, A45
 Fujiwara, H., Onaka, T., Ishihara, D., et al. 2010, *ApJL*, **714**, L152
 Fujiwara, H., Onaka, T., Yamashita, T., et al. 2012, *ApJL*, **749**, L29
 Gail, H.-P. 2002, *A&A*, **390**, 253
 Genda, H., Kobayashi, H., & Kokubo, E. 2016, *ApJ*, **810**, 136
 Green, J. D., Hartmann, L., Calvet, N., et al. 2006, *ApJ*, **648**, 1099
 Green, J. D., Jones, O. C., Keller, L. D., et al. 2016, *ApJ*, **832**, 4
 Guinan, E. F., & Engle, S. G. 2007, arXiv:0711.1530
 Gunther, M. N., Zhan, Z., Seager, S., et al. 2020, *AJ*, **159**, 60
 Hartmann, L., & Kenyon, S. J. 1996, *A&A*, **34**, 207
 Herter, T., Campins, H., & Gull, G. E. 1987, *A&A*, **187**, 629
 Honda, M., Katata, H., Okamoto, Y., et al. 2004, *ApJL*, **610**, L49
 Houck, J. R., Roellig, T. L., van Gleeve, J., et al. 2004, *ApJS*, **154**, 18
 Hubbard, A. 2017, *ApJL*, **840**, L5
 Husser, T.-O., Wende-von Berg, S., Dreizler, S., et al. 2013, *A&A*, **553**, A6
 Jackson, A. P., & Wyatt, M. C. 2012, *MNRAS*, **425**, 657
 Johnson, B. C., Lisse, C. M., Chen, C. H., et al. 2012, *ApJ*, **761**, 45
 Jura, M., Fahiri, J., Zuckerman, B., & Becklin, E. 2007, *AJ*, **133**, 1927
 Kennedy, G. M., Murphy, S. J., Lisse, C. M., et al. 2014, *MNRAS*, **438**, 3299
 Kenyon, S. J., & Bromley, B. C. 2005, *AJ*, **130**, 269
 Kenyon, S. J., & Bromley, B. C. 2006, *AJ*, **131**, 1837
 Kenyon, S. J., & Bromley, B. C. 2016, *ApJ*, **817**, 51
 Koeberl, C. 1988, *Metic*, **23**, 161
 Kohout, T., Malina, O., Penttilä, A., et al. 2014, *Icar*, **237**, 75
 Kohout, T., Malina, O., Penttilä, A., et al. 2016, *LPI*, **47**, 2042
 Kokubo, E., & Genda, H. 2010, *ApJL*, **714**, L21
 Kokubo, E., & Ida, S. 1998, *Icar*, **131**, 171
 Kraus, S., Ireland, M. J., Sitko, M. L., et al. 2013, *ApJ*, **768**, 80
 Lammer, H., Selsis, F., Ribas, I., et al. 2003, *ApJL*, **598**, L121
 Leboutteiller, V., Barry, D. J., Goes, C., et al. 2015, *ApJS*, **218**, 21
 Leboutteiller, V., Barry, D. J., Spoon, H. W. W., et al. 2011, *ApJS*, **196**, 8
 Lévasseur-Regourd, A. C., Agarwal, J., & Cottin, H. 2018, *SSRv*, **214**, 64
 Lieman-Sifry, J., Hughes, A. M., Carpenter, J. M., et al. 2016, *ApJ*, **828**, 1
 Lisse, C. M., Beichman, C. A., Bryden, G., & Wyatt, M. C. 2007a, *ApJ*, **658**, 584
 Lisse, C. M., Chen, C. H., Wyatt, M. C., & Morlok, A. 2008, *ApJ*, **673**, 1106
 Lisse, C. M., Chen, C. H., Wyatt, M. C., et al. 2009, *ApJ*, **701**, 2019
 Lisse, C. M., Christian, D. J., Wolk, S. W., et al. 2017a, *AJ*, **153**, 62
 Lisse, C. M., Kraemer, K. E., Nuth, J. A., Li, A., & Joswiak, D. 2007b, *Icar*, **187**, 69
 Lisse, C. M., Sitko, M. L., & Marengo, M. 2015, *ApJL*, **815**, L27
 Lisse, C. M., Sitko, M. L., & Marengo, M. 2017b, *AJ*, **154**, 182
 Lisse, C. M., Sitko, M. L., Russell, R. W., et al. 2017c, *ApJL*, **840**, L20
 Lisse, C. M., van Cleve, J., Adams, A. C., et al. 2006, *Sci*, **313**, 635
 Lisse, C. M., Wyatt, M. C., Chen, C. H., et al. 2012, *ApJ*, **747**, 93
 Mamajek, E. 2009, in AIP Con. Ser. 1158, Exoplanets and Disks: Their Formation and Diversity, ed. T. Usuda, M. Tamura, & M. Ishii (Melville, NY: AIP), 3
 Mamajek, E. E., & Bell, C. P. M. 2014, *MNRAS*, **445**, 2169
 Mannel, T., Bentley, M. S., & Boakes, P. D. 2019, *A&A*, **630**, A26
 Meng, H. Y. A., Rieke, G. H., Su, K. Y. L., & Gáspár, A. 2017, *ApJ*, **836**, 34
 Meng, H. Y. A., Su, K. Y. L., Rieke, G. H., et al. 2014, *Sci*, **345**, 1032
 Meng, H. Y. A., Su, K. Y. L., Rieke, G. H., et al. 2015, *ApJ*, **805**, 77
 Mittal, T., Chen, C. H., Jang-Condell, H., et al. 2015, *ApJ*, **798**, 87
 Morishima, R., Stadel, J., & Moore, B. 2010, *Icar*, **207**, 517
 Nuth, J. A., & Johnson, N. M. 2006, *Icar*, **180**, 243
 Olofsson, J., Juhász, A., Henning, T., et al. 2012, *A&A*, **542**, 90
 Osten, R. A., & Wolk, S. J. 2015, *ApJ*, **809**, 79
 Paczynski, B. 2000, *PASP*, **112**, 1281
 Pantín, E., & Di Folco, E. 2011, EPSC-DPS2011-825
 Panzera, M. R., Tagliaferri, G., Pasinetti, L., & Antonello, E. 1999, *A&A*, **348**, 161
 Pecaut, M. J., & Mamajek, E. E. 2013, *ApJS*, **208**, 9
 Pecaut, M. J., Mamajek, E. E., & Bubar, E. J. 2012, *ApJ*, **746**, 154
 Pieters, C. M., & Noble, S. K. 2016, *JGRE*, **121**, 1865
 Pojmanski, G. 2002, *AcA*, **52**, 397
 Pojmanski, G., & Maciejewski, G. 2004, *AcA*, **54**, 153
 Preibisch, T., & Mamajek, E. 2008, in Handbook of Star-forming Regions Vol. II, ed. B. Reipurth (San Francisco, CA: ASP), 235
 Quader, A. H., Pacheco, S., Au, A., et al. 2015, *JGRE*, **120**, 643
 Raymond, S. N., Armitage, P. J., Moro-Martín, A., et al. 2011, *A&A*, **530**, 62
 Raymond, S. N., Kokubo, E., Morbidelli, A., Morishima, R., & Walsh, K. J. 2014, in Protostars and Planets VI, ed. H. Beuther et al. (Tucson: Univ. Arizona Press), 595
 Reach, W. T., Lisse, C. M., von Hippel, T., & Mulally, F. 2009, *ApJ*, **693**, 1
 Reach, W. T., Vaubaillon, J., Lisse, C. H., Holloway, M., & Rho, J. 2010, *Icar*, **208**, 276
 Reddy, V., Nathues, A., Le Corre, L., et al. 2012, *Sci*, **336**, 700
 Reegen, P. 2007, *A&A*, **467**, 1353
 Rhee, J. H., Song, I., & Zuckerman, B. 2007, *ApJ*, **671**, 616
 Rhee, J. H., Song, I., & Zuckerman, B. 2008, *ApJ*, **675**, 777
 Ribas, Á., Bouy, H., & Merín, B. 2015, *A&A*, **576**, 52
 Ribas, I., Guinan, E. F., Güdel, M., & Audard, M. 2005, *ApJ*, **622**, 680
 Ricker, G., Winn, J. N., Vanderspek, R., et al. 2015, *JATIS*, **1**, 014003
 Ruff, S. W., Farmer, J. D., Calvin, W. M., et al. 2011, *JGRE*, **116**, E00F23
 Sargent, B., Forrest, W. J., D'Allesio, P., et al. 2006, *ApJ*, **645**, 395
 Schelling, P. K., Britt, D. T., Quader, A. H., et al. 2015, *LPICo*, **1878**, 2052
 Schmitt, J. H. M. M., & Liefke, C. 2004, *A&A*, **417**, 651
 Sitko, M. L., Lisse, C. M., Kelley, M. S., et al. 2011, *AJ*, **142**, 80
 Speck, A. K., Whittington, A. G., Hofmeister, A. N., et al. 2011, *ApJ*, **740**, 93
 Suchkov, A. A., Makarov, V. V., & Voges, W. 2003, *ApJ*, **595**, 1206
 Sylvester, R. J., & Mannings, V. 2000, *MNRAS*, **313**, 73
 Takasawa, S., Nakamura, A. M., Kadono, T., et al. 2011, *ApJL*, **733**, 2
 Van Doorselaere, T. V., Shariati, H., & Debusscher, J. 2017, *ApJS*, **232**, 26
 Watson, D. M., Leisenring, J. M., Furlan, E., et al. 2009, *ApJS*, **180**, 84
 Weinberger, A. J., Becklin, E. E., Song, I., & Zuckerman, B. 2011, *ApJ*, **726**, 72
 Westphal, A. J., Bridges, J. C., & Brownlee, D. E. 2017, *M&PS*, **52**, 1859
 Wilson, T. L., Nilsson, R., Chen, C. H., et al. 2016, *ApJ*, **826**, 165
 Wooden, D. H., Ishii, H. A., & Zolensky, M. E. 2017, *RSPTA*, **375**, 20160260
 Wright, N. J., Drake, J. J., Mamajek, E. E., & Henry, G. W. 2011, *ApJ*, **743**, 48
 Zolensky, M. E., Gounelle, M., Briani, G., et al. 2008, *M&PSA*, **43**, 5265
 Zuckerman, B., & Song, I. 2004, *ApJ*, **603**, 738